



January 2013

Targeted Overexpression Of Metallothionein In Endothelial Cells Mitigates Pulmonary Alveolar Basement Membrane Thickening In Transgenic Diabetic Ove Mice: An Unbiased Tem Morphometric Analysis

Holly M. Hewitt

Follow this and additional works at: <https://commons.und.edu/theses>

Recommended Citation

Hewitt, Holly M., "Targeted Overexpression Of Metallothionein In Endothelial Cells Mitigates Pulmonary Alveolar Basement Membrane Thickening In Transgenic Diabetic Ove Mice: An Unbiased Tem Morphometric Analysis" (2013). *Theses and Dissertations*. 1542.

<https://commons.und.edu/theses/1542>

This Thesis is brought to you for free and open access by the Theses, Dissertations, and Senior Projects at UND Scholarly Commons. It has been accepted for inclusion in Theses and Dissertations by an authorized administrator of UND Scholarly Commons. For more information, please contact zeinebyousif@library.und.edu.

TARGETED OVEREXPRESSION OF METALLOTHIONEIN IN ENDOTHELIAL
CELLS MITIGATES PULMONARY ALVEOLAR BASEMENT MEMBRANE
THICKENING IN TRANSGENIC DIABETIC OVE MICE: AN UNBIASED TEM
MORPHOMETRIC ANALYSIS

by

Holly M. Hewitt
Bachelor of Arts, Concordia College, 2010

A Thesis

Submitted to the Graduate Faculty

of the

University of North Dakota

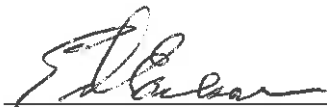
in partial fulfillment of the requirements

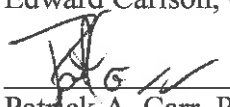
for the degree of

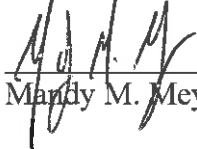
Master of Science

Grand Forks, North Dakota
December
2013

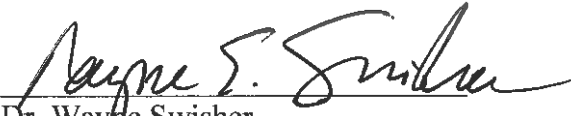
This thesis, submitted by Holly M. Hewitt in partial fulfillment of the requirements for the Degree of Master of Science from the University of North Dakota, has been read by the Faculty Advisory Committee under whom the work has been done and is hereby approved.

 12/4/13
Edward Carlson, Chairperson

 12/4/13
Patrick A. Carr, PhD

 12/4/13
Mandy M. Meyer, PhD

This thesis is being submitted by the appointed advisory committee as having met all of the requirements of the School of Graduate Studies at the University of North Dakota and is hereby approved.


Dr. Wayne Swisher
Dean, School of Graduate Studies


Date

PERMISSION

Title: Targeted Overexpression of Metallothionein in Endothelial Cells
Mitigates Pulmonary Alveolar Basement Membrane Thickening in
Transgenic Diabetic OVE Mice: An Unbiased TEM Morphometric
Analysis

Department: Anatomy and Cell Biology

Degree: Master of Science

In presenting this thesis in partial fulfillment of the requirements for a graduate degree from the University of North Dakota, I agree that the library of this University shall make it freely available for inspection. I further agree that permission for extensive copying for scholarly purposes may be granted by the professor who supervised my thesis work, or in their absence, by the chairperson of the department or the dean of the School of Graduate Studies. It is understood that any copying or publication or other use of this thesis or part thereof for financial gain shall not be allowed without my written permission. It is also understood that due recognition shall be given to me and to the University of North Dakota in any scholarly use which may be made of any material in my thesis.

Holly M. Hewitt
November 21, 2013

TABLE OF CONTENTS

| | |
|--|------|
| LIST OF FIGURES | vii |
| LIST OF TABLES | viii |
| ACKNOWLEDGMENTS | ix |
| ABSTRACT..... | xii |
| CHAPTER | |
| I. INTRODUCTION | 1 |
| Chronic Complications of Diabetes Mellitus..... | 3 |
| The Extracellular Matrix and Diabetic Induced Alterations..... | 4 |
| Hyperglycemia and Reactive Oxygen Species | 6 |
| Antioxidant Therapy and Protection against Basement Membrane Thickening | 9 |
| Histology of Pulmonary Tissue | 13 |
| Objectives of Current Study..... | 16 |
| II. MATERIALS AND METHODS..... | 18 |
| Research Animals | 18 |
| Genotyping..... | 19 |
| Quantification of MT in Pulmonary Tissues | 21 |
| Vascular Perfusion and Tissue Preparation of Microtomy | 23 |
| Statistics | 31 |

| | | |
|------|--|----|
| III. | RESULTS | 32 |
| | General Condition of Animals | 32 |
| | Pulmonary Morphology | 33 |
| | Pulmonary Alveolar Basement Membrane (PABM) Morphometry | 36 |
| | Analysis of MTI/II Expression | 37 |
| IV. | DISCUSSION | 39 |
| | APPENDIX..... | 47 |
| | REFERENCES | 64 |

LIST OF FIGURES

| Figure | Page |
|---|------|
| 1. General appearance of 150 day-old mice..... | 49 |
| 2. Toluidine blue stained light micrograph with higher magnification transmission electron micrograph inset of terminal respiratory region of 150 day-old FVB control mouse lung..... | 50 |
| 3. Transmission electron micrograph of 150 day-old FVB control mouse lung | 52 |
| 4. Transmission electron micrograph of two adjacent respiratory filtration barriers in lung of 150 day-old FVB control mouse | 53 |
| 5. Representative transmission electron micrographs of respiratory filtration barriers in 60 day-old FVB, Jtmt, OVE, and OVEJtmt mice | 54 |
| 6. Representative transmission electron micrographs of respiratory filtration barriers in 150 day-old FVB, Jtmt, OVE, and OVEJtmt mice | 56 |
| 7. Mean pulmonary alveolar basement membrane thickness in 60 day-old mice..... | 58 |
| 8. Mean pulmonary alveolar basement membrane thickness in 150 day-old mice..... | 59 |
| 9. Age-related mean pulmonary alveolar basement membrane thickness in 60 day-old and 150 day-old mice..... | 60 |
| 10. Representative light micrographs of paraffin embedded kidney cortex and lung immunohistochemically stained for MTII | 61 |
| 11. Average pulmonary MTII $\mu\text{g}/\text{mg}$ total tissue protein) in FVB control (n=2), Jtmt transgenic (n=2), OVE (n=2) and OVEJtmt (n=2) transgenic and bi-transgenic animals $\pm\text{S.D.}$ | 63 |

LIST OF TABLES

| Table | | Page |
|-------|--|------|
| 1. | Animal genotype, number of animals, number of epoxy blocks sectioned, number of micrographs taken, and number of measurements made per micrograph for orthogonal intercept calculation of true PABM thickness..... | 48 |
| 2. | Mean body weight, blood glucose, and HbA1c values from 60 and 150 day-old FVB, Jtmt, OVE and OVEJtmt mice \pm S.D..... | 49 |
| 3. | Age-related mean pulmonary alveolar basement membrane thickness in 60 and 150 day-old mice..... | 60 |

ACKNOWLEDGMENTS

I have many people to thank for helping me throughout my years as a graduate student. For the continuous support and encouragement from family, friends, faculty, and colleagues, I thank you from the bottom of my heart. You have helped me endure the rough patches, but more importantly, celebrate my achievements in graduate school.

I would like to express my sincere gratitude to my advisor, Dr. Edward Carlson. You have been the kindest and most genuine role model I could have ever asked for. Without you, I would not have been able to complete my degree and I sincerely appreciate your taking a chance on me. You have provided me with guidance every step of the way while also allowing me freedom to grow on my own. Your confidence in me has provided me the foundation I needed to have confidence in myself. I will never forget your tenacity and excitement for science, fortitude in mentoring students, and optimistic approach in everything you encounter, all of which I will bring with me on my future endeavors. Thank you.

Thank you, Drs. Pat Carr and Mandy Meyer. You have been wonderful committee members and I appreciate you taking the time out of your busy lives to provide me with advice, guidance, and support. You are both fantastic educators that I look up to and I hope someday to be even half the instructors that you are. Thank you for your time, patience, and leadership.

Were it not for my parent's encouragement to be curious and investigate from a young age, I would not have developed the scientific inquiry that I possess today. Their

continual support throughout my years of schooling has gotten me here today, and to them, I owe everything.

To my husband, Tony Hewitt, thank you for studying chemistry with me in our undergraduate education and deciding that we were such good study partners, we should get married. I would not have been able to succeed and complete as many goals as I have without your encouragement and faith in me. Words will never be able to express how much your love and support have meant to me.

To Donna Latus, thank you for having such a kind heart and sharing it with everyone you meet. Because of you, from my very first day in lab, I have always felt at home. You have provided me with a genuine friendship that I will always cherish. Additionally, I have you to thank for teaching me so many techniques in the lab that were not only essential for my project, but for future experiences as well.

To Dr. John Swinscoe, thank you for help with the ELISA protocol and having patience with me when showing me laboratory techniques. I also appreciate your feedback and advice throughout the past year, I've learned so much.

I would also like to express my gratefulness to Kim Young and Bonnie Kee. You have both been so helpful in anything and everything that I have needed. Kim, your eagerness to assist me with integral parts of many experiments has helped me accomplish many goals and meet numerous deadlines. I am thankful of your kind heart and greatly appreciate your help. Bonnie, you have assisted me, even with only a moment's notice, with critical aspects of my graduate education, including formatting this thesis. I appreciate everything you have done and the patience you have shown me. Without you, I would not have been able to graduate. You deserve so much recognition for your hard

work and dedication not only to the University, but also to the students, faculty, and staff.

Thank you for all that you do.

ABSTRACT

Damage to small blood vessels in diabetes mellitus (DM) is largely the result of hyperglycemia-driven oxidative stress. This is manifested morphologically by capillary basement membrane (BM) thickening, the hallmark feature of chronic complications of DM. In an effort to demonstrate pulmonary alveolar BM (PABM) thickness increase in DM and to demonstrate for the first time, mitigation of the increase utilizing antioxidant therapy, we crossed the severely diabetic transgenic mouse (OVE) with Jtmt, our recently developed transgenic animal model that overexpresses the antioxidant metallothionein (MT) in endothelial cells. Unbiased TEM morphometry demonstrated that PABM widths in diabetic (OVE) mice were significantly (+20%) thickened. Remarkably, however, the bi-transgenic OVEJtmt progeny exhibited statistically significant protection against DM-derived BM thickening. These results provide evidence for a direct role of oxidative damage to endothelial cells in diabetic mice and show that protection of these cells can reduce one of the primary features of diabetic microangiopathy.

CHAPTER I

INTRODUCTION

Diabetes mellitus (DM) is a serious and potentially debilitating disease that is considered an epidemic in the Western hemisphere including the United States where approximately 8.3% of the population is diabetic (Center for Disease Control, 2011). In 2000, more than 171 million people were afflicted with the disease worldwide and it is anticipated that by the year 2030, more than 366 million people will be diagnosed (Wild et al., 2004; WHO, 2006). Importantly, by 2030, DM is predicted to be the seventh leading cause of death in the U.S. due to the serious vascular complications that accompany it (WHO, 2006). Extensive research has been carried out in an effort to eliminate DM and to mitigate its chronic complications. Nevertheless, additional studies will be required to understand the causes of DM and reduce the escalating number of diagnoses and increased health care costs each year.

Diabetes is characterized as a group of metabolic diseases, in which hyperglycemia and glucose intolerance transpire, which results in diseased microvasculature. The two main types of DM are Type I (T1D) and Type II (T2D). Each is characterized by chronic hyperglycemia as well as deregulated metabolism of fats, proteins, and carbohydrates (McCance and Heuther, 2010).

Type I DM is an autoimmune condition caused by malfunctioning primary pancreatic beta cells. This condition is also known as Insulin-Dependent Diabetes (IDD)

because the pancreas produces and secretes insufficient amounts of insulin (Jahromi and Eisenbarth, 2007). Accordingly, diabetic patients depend on synthetic insulin for maintenance of appropriate serum blood sugar and survival (Jahromi and Eisenbarth, 2007). Type I diabetes accounts for approximately 10% of all diagnosed cases, and its incidence has nearly doubled over the past twenty years (Nokoff and Rewers, 2013). In the United States, individuals under the age of 20 are especially at risk of developing T1D, as shown by an increase in diagnoses in this age group by 23% between 2001 and 2009 (Nokoff and Rewers, 2013). It is hypothesized that this increase is correlated to the epidemic of childhood obesity.

Within the Type I class, there are two subcategories: autoimmune diabetes [type 1A (T1A)] and nonimmune diabetes [type 1B (T1B)] (Jahromi and Eisenbarth, 2007). Type 1B diabetes, also known as idiopathic diabetes, often occurs as a secondary condition initiated by other ailments affecting the pancreas, such as pancreatitis, neoplasia, and cystic fibrosis (McCance and Heuther, 2010). Type 1A diabetes is more common than T1B and is triggered by a combination of genetic and environmental factors resulting in the overproduction of autoantibodies that destroy pancreatic beta cells (Jahromi and Eisenbarth, 2007).

Environmental factors that have been strongly correlated with the cause of T1D include viral infections such as: mumps, enteroviruses, endogenous retroviruses, parvovirus, rotovirus, cytomegalovirus, and congenital rubella (Richer and Horwitz, 2008), drugs and chemicals such as: streptozotocin, alloxan, pentamidine, and vacor, (McCance and Heuther, 2010) and dietary factors such as, bovine milk and cereal (Jahromi and Eisenbarth, 2007).

In addition to environmental contributors, a strong link between specific genetic backgrounds and the development of autoimmune diseases, including T1D, have been made. The histocompatibility leukocyte antigen (HLA) and its associated genetic variants have been the most compelling risk factor in familial diabetic cases (Nokoff and Rewers, 2013).

Type II diabetes is by far the most common type of diabetes, and accounts for 90-95% of diagnosed cases (Nokoff and Rewers, 2013). Onset of T2D often occurs later in life, with an average age between 45-64 years. Incidence rates are increasing in all age groups in the United States, and the risk of developing the disease increases after the age of 40 (McCance and Heuther, 2010). Obesity significantly increases the risk for developing the disease and the risk is related to the duration, degree, and distribution of obesity (McCance and Heuther, 2010). The major distinction between T2D and T1D is the development of insulin resistance in T2D, as well as decreased insulin secretion over the duration of the illness (Wright et al., 2006).

Genetic predisposition, age, and other environmental factors contribute to the risk of developing DM and treating its inevitable complications is essential. The pathophysiology of these complications must be understood because the increasing morbidity and mortality of DM is caused by the associated chronic complications in the macro- and microvasculature (Sheetz, 2002).

Chronic Complications of Diabetes Mellitus

Insulin resistance and chronic hyperglycemia have been implicated in the pathogenesis of chronic complications associated with DM (Brownlee, 2001). Chronic complications of DM are serious pathological states associated with the condition that

contribute to significantly increased health care costs and major obstacles in diabetes therapy. The most common chronic complications include; diabetic nephropathy, diabetic cardiomyopathy, diabetic neuropathy, and diabetic retinopathy.

Macrovascular complications occur when arteries supplying the brain, heart, and lower extremities become atherosclerotic (Brownlee, 2001). Diseased large vessels contribute to the fact that diabetic patients have an increased incidence of myocardial infarction, stroke, and lower limb amputation (Brownlee, 2001). Microvascular complications are pathological states of smaller blood vessels supplying the retina, kidneys, and peripheral nerves. Atherosclerotic microvasculature is a major cause of blindness, end stage renal disease, and peripheral nerve damage in many diabetic patients (Brownlee, 2001).

Interestingly, a unifying pathophysiological change in these chronic complications is the thickening of basement membranes (BM) - a specialized component of the extracellular matrix (ECM) associated with all non-connective tissues including the endothelium of the macro- and microvasculature (Ozsahin et al., 2006).

The Extracellular Matrix and Diabetic Induced Alterations

The ECM is a biophysical component of cellular networks that maintains structural and mechanical properties of the cells (Smits et al., 2010). It not only has roles in maintaining the structure of the cellular network, but also in signaling cascades for the proper functioning of cells. Fibrous proteins that comprise the ECM are located between clusters of cells within all tissue and provide tensile strength, routes for communication, and movement of cells within tissues (Kalluri, 2003).

Basement Membranes

Basement membranes are specialized ECM ranging between 50-350 nm in thickness and are synthesized by epithelial cells (Kalluri, 2003). They are arranged as a sheet-like structure located between cells, cell surfaces, and the interstitium, serving as a partition between cell monolayers and the connective tissue space (Yurchenco, 2009). Cell monolayers produce and secrete specialized glycoproteins that form the BM on their basolateral surfaces (Yurchenco, 2009). Epithelia (including the endothelium) throughout the entire body are in direct association with BMs for tissue organization, structural support, and regulation in cellular signaling (Kalluri, 2003).

The biochemical composition of BMs varies from tissue to tissue and these differences are due to tissue-specific expression of protein isoforms, alternative splicing, and posttranslational modifications (LeBleu, 2007). Composition of BMs can also be relatively dynamic based on the physiologic or pathophysiologic state of tissues (LeBleu et al., 2007). Despite the heterogeneous expression of these molecules in tissues, there are several proteinaceous components found universally in BMs.

Collagen (type IV), laminin, nidogen/entactin, and heparan sulfate proteoglycans (perlecan and agrin) comprise the majority of BM molecules and are intricately involved in its functions (Yurchenco, 2009). These proteins are extensively coupled to other molecules involved in signaling cascades that control cell motility, differentiation, the cell cycle, and the expression of other genes and proteins (Yurchenco, 2009).

Alterations in BM

Thickening of the BM, especially in the kidney, is a primary pathophysiological feature found in DM patients and is a hallmark of the disease (Bergstrand and Bucht,

1959). The hyperglycemic environment present in DM antagonizes the homeostatic nature of cells, which activates a biological stress response. One consequence of a cellular stress response is the potential alteration of BM composition (Rohrbach and Martin, 1982).

One of the first diabetic induced alterations of BMs reported was in the kidney (Kimmelstiel and Wilson, 1936). Within the renal glomerular mesangium, a network of mesangial cells (intercapillary cells) and mesangial matrix provide mechanical support for glomerular capillaries (Suzuki et al., 1963). The renal mesangial cells respond to injury, by cellular proliferation and increased deposition of matrix molecules, known pathologically as Kimmelstiel-Wilson nodules. These are observed in patients with diabetic nephropathy (Suzuki et al., 1963). Diabetic nephropathy is characterized by increased deposition of ECM proteins in the mesangium as well as BM thickening in the glomerulus (Mason and Wahab, 2003).

It is widely accepted that increased synthesis of ECM molecules in DM is a result of the activation of several pathways, leading to either the increased synthesis of ECM proteins and/or the decreased degradation of aged ECM proteins (i.e. decreased ECM turnover).

Hyperglycemia and Reactive Oxygen Species

Hyperglycemia has been shown to cause adverse effects on many biochemical pathways in vascular tissues and one of these consequences is the excess production of reactive oxygen species (ROS) which contributes to increased cellular and extracellular oxidative stress (Son, 2007). In general, cells respond to this stress by activating various intracellular signaling pathways, and consequently, gene activation (Son, 2007).

Hyperglycemia-induced intracellular signaling has been shown to contribute to BM thickening in most tissues through pathways activated by the presence of ROS (Sheetz, 2002). Increased levels of ROS in T1D and T2D transpire through a series of complex and intertwined molecular pathways.

Reactive oxygen species, at moderate levels, are involved in various molecular mechanisms and signaling pathways to produce normal cellular responses. The oxidation of water, or reduction of molecular oxygen, to give products such as superoxide anion (O_2^-), hydrogen peroxide (H_2O_2) and hydroxyl radical ($+OH$) in the mitochondria provide biological systems with the majority of ROS (Rains et al., 2011). When ROS are present in higher than normal amounts, detrimental consequences to cells, including lipid membrane destruction, oxidative damage to DNA, excess cross-linking of proteins, and inappropriate activation of stress related signaling pathways could disrupt cell behavior (Son, 2007).

The mechanisms behind hyperglycemia-induced vascular damage are largely driven by the action of ROS. Theories involving four molecular pathways are recognized in causing glucose-mediated vascular damage, including, the aldose reductase (polyol pathway) theory, activation of protein kinase C (PKC) isoforms, the reactive oxygen intermediate theory, and increased intracellular formation of advanced glycation end-products (AGEs) (Sheetz, 2002).

The aldose reductase (polyol pathway) mechanism is activated when intracellular glucose concentrations are elevated (Sheetz, 2002). Aldose reductase is an enzyme that utilizes nicotinamide adenine dinucleotide phosphate (NADPH) as a reducing agent in the conversion of glucose to sorbitol (Madonna, 2011). As a result of the increase of

aldose reductase in endothelial cells, sorbitol is oxidized by sorbitol dehydrogenase, leading to the production of fructose (Sheetz, 2002). This process occurs with the coupled reduction of NAD⁺ to NADH (Sheetz, 2002). Overall, the increased activity of aldose reductase and reduced levels of NADPH causes downstream disturbance of the redox balance within the vascular tissues (Sheetz, 2002).

Activation of PKC isoforms is also intricately involved in the development of diabetic vascular complications. In hyperglycemic environments, PKC is activated and is able to alter cellular behavior in various ways. Intracellular hyperglycemic environments trigger the activation of a second messenger, diacylglycerol (DAG) (Madonna, 2011). In endothelial cells, DAG activates PKC, which triggers intracellular events to alter gene expression. Specifically, PKC activation leads to BM thickening by the activation of transforming growth factor (TGF) β , collagen, and fibronectin (Madonna, 2011). In addition to the activation of DAG, elevated glucose concentrations increase overall glycolytic pathway activity and the levels of glyceraldehyde-3-phosphate (GAP) inside endothelial cells (Sheetz, 2002). Oxidative phosphorylation of GAP contributes to the activation of reactive oxygen intermediates (ROI), initiating an oxidative stress response of vascular endothelial cells (Sheetz, 2002).

The ROI pathway directly contributes to the oxidative environment of endothelial cells and vascular damage through several mechanisms, including oxidative phosphorylation of GAP in the previously described PKC signaling pathway. An increase in glucose metabolism through the glycolytic pathway and the tricarboxylic acid cycle (TCA) increases mitochondrial adenosine triphosphate (ATP) synthesis by oxidative phosphorylation (Nishikawa, 2000). Several byproducts of this biochemical process

include free radicals, such as the superoxide anion. Increased levels of superoxide anion, as previously discussed, generates an oxidative environment and stress on vascular tissue, ultimately leading to cellular damage and altered cellular behavior.

A fourth mechanism involved in the development of diabetic chronic complications is the AGE pathway. Advanced glycation end products are proteins that become altered, and irreversibly modified, in the normal course of aging (Sheetz, 2002). Increased levels of glucose cause additional covalent modifications and crosslinking of proteins and in diabetics this process has been described as a process of accelerated aging (Monnier, 1984). Further cellular dysfunction and vascular damage occur by AGEs binding receptors to advanced glycation end products (RAGE) (Goh and Cooper, 2008). When these transmembrane receptors are activated, additional signaling events are also initiated, such as the activation of mitogen-activated protein kinase (MAP) pathway, which leads to endothelial cell dysfunction (Schmidt, 2000).

A common relationship exists between these four pathways; they are all initiated by hyperglycemia and their activation results in an overproduction of superoxide, which has been strongly associated with hyperglycemia-induced oxidative stress responses in diabetics (Madonna, 2011). Although it remains unclear as to which mechanism is the primary source of hyperglycemia-induced production of ROS, it could be the combination of these pathways that contribute to vascular complications (Velic et al, 2013).

Antioxidant Therapy and Protection against Basement Membrane Thickening

The overproduction of free radicals in diabetics is initiated through glucose oxidation, nonenzymatic glycation of proteins, and oxidative degradation of glycated

proteins (Cai, 2004). One way of neutralizing diabetic oxidative damage, and the consequences of oxidative stress (BM thickening), is through the protective properties of antioxidants.

In this regard, one of the most potent antioxidants referenced in the literature is metallothionein (MT). Metallothioneins are a family of proteins known to bind to metals, such as zinc (Zn), cadmium (Cd), copper (Cu), and iron (Fe) and cysteine-rich residues in cells (Cai, 2004). There are at least ten known isoforms of MT in humans and they are further classified into major and minor groups (Thirumoorthy et al., 2011).

Metallothionein isoforms have a wide range of protective characteristics, offering scavenging against free radicals such as the hydroxyl radical and peroxynitrite, which are considered the most active radicals (Cai, 2004). Due to its various protective properties and global expression throughout the body, MT isoforms I and II (MTI/II) comprise the major group of MTs (Thirumoorthy et al., 2011). As a scavenger of various radicals, MT has been shown to be >50 times more powerful than other antioxidants, and thus, MT offers promising protective properties against oxidative stress-related damage in cells and tissues of diabetic patients (Kumari et al., 1998).

Antioxidant Therapy

Antioxidant therapy has been studied in various animal models to counterbalance the overproduction of ROS in diabetic and insulin-resistant mice (Son, 2007). One such mouse, the OVE26 (herein referred to as OVE), is a transgenic diabetic mouse that has been shown to be a valuable model of human type I DM (Zheng et al., 2008). The OVE mouse was developed by introducing a minigene to overexpress calmodulin in the pancreatic beta cell (Epstein et al., 1989). Overexpression of calmodulin in the beta cell

interrupts the physiological response of these cells to produce and secrete insulin. This interruption of insulin production makes the OVE mouse an excellent model to study the genetic background of insulin secretion (Epstein et al., 1992). These transgenic mice can easily be identified by the phenotypic marker, small eyes. The presence of small eyes is caused by the intentional cointegration of the GR19 gene (Liang et al., 2002). The OVE mouse is maintained on the Friend virus B-type susceptibility (FVB) background. The FVB mice are an inbred mouse strain maintained by the National Institutes of Health (NIH) for studying transgenic mice (Taketo et al., 1991).

With the establishment of a reliable mouse model that demonstrates common characteristics of human DM, it is possible to study the effects of antioxidant therapy. Recent studies utilizing these diabetic and transgenic mouse models provide evidence that oxidative stress in diabetics can be mitigated. In 2003, Carlson and co-workers carried out morphometric analyses of capillary BM thickness in various tissues in 350 day-old OVE diabetic and normal FVB mice. Interestingly, in addition to the renal glomerulus, several other tissues were susceptible to hyperglycemia-induced capillary BM thickening. These included skeletal and cardiac muscle, retina and choroid, peripheral nerve, lung, and pancreas (Carlson et al., 2003). Not surprisingly, the renal glomerulus and ocular retina exhibited the highest susceptibility to BM thickening in diabetic mice. However, the lung and respiratory diaphragm also demonstrated significant capillary BM thickening in OVE transgenic diabetic mice.

Early work with the OVE mouse and potential antioxidant protection against BM thickening was conducted with the development of a transgenic mouse that overexpressed MT in myocardial cells (Mt) (Liang et al., 2002). Progeny of the OVE and

Mt mice showed significant reduction in myocardial oxidative damage and decreased myocardial capillary BM thickening in transgenic diabetic mice. Furthermore, targeted overexpression of MT provided antioxidant protection against oxidative stress in cardiac myocytes and also protected against diabetic cardiomyopathy (Velic et al., 2013).

Metallothionein also has been targeted to other cells in efforts to study its protective properties against diabetic nephropathy (DN). The Nmt transgenic mouse overexpresses MT in the podocytes of the kidney (Zheng et al., 2008). Moreover, progeny of OVE and Nmt mice show significant protection against DN and associated glomerular injury (Carlson et al., 2013). Severe albuminuria, glomerular filtration barrier damage, and changes in glomerular endothelial and mesangial cell numbers are all consequences of DN, and all are reduced by the presence of targeted MT in podocytes (Carlson et al., 2013).

Overexpression of MT in cardiac myocytes and renal podocytes strongly supported the theory of antioxidant therapy in treating oxidative stress related damage to these specific tissues. This stimulated a number of investigators to begin efforts toward building a transgenic mouse that overexpressed MT in endothelial cells, a cell type ubiquitously distributed with the macro- and microvasculature. Accordingly, the endothelial cell, appropriately armed with overexpressed MT could show the potential to reduce vascular BM thickening globally.

Jtmt Mice

To test the hypothesis of antioxidant protection against diabetes-induced oxidative damage in other tissues, the human *MTII* gene needed to be introduced, universally, into endothelial cells. In response to this requisite, a *Jtmt* transgene was designed and purified

by Teiken (2011) to overexpress the human MTII gene, and the purified *Jtmt* transgene was inserted into the developing zygote (into the pronucleus) of FVB mouse embryos (Transgenic Mouse Laboratory, Children's Hospital Research Foundation of Cincinnati).

The *Jtmt* transgene was inserted into the pHHNS plasmid, which contains the *Tie2* promoter and enhancer for murine endothelial cells. The *Tie2* promoter and enhancer ensured that the *Jtmt* gene would be expressed specifically in the endothelium, thus creating the *Jtmt* mouse line (Teiken, 2011).

The establishment of a transgenic mouse that overexpresses MT universally in its endothelial cells provides a unique vehicle to study antioxidant protection in a wide variety of tissues in control and transgenic mouse models. One such tissue, the lung, is a particularly appropriate candidate for experimentation. As mentioned earlier, the lung is susceptible to hyperglycemia-induced significant BM thickening (Carlson et al., 2003). Its similar structural arrangement to the glomerular filtration barrier in the kidney could offer insight into the specific cellular mechanisms in BM thickening of each tissue. Additionally, as the largest microvascular structure in the body (Shafiee et al., 2013), the lung warrants further exploration into potential chronic diabetic pulmonary complications, specifically any morphological alterations in the pulmonary alveolar basement membrane (PABM).

Histology of Pulmonary Tissue

The respiratory system is divided into two functional parts; the conducting portion and the respiratory portion. The conducting portion includes the air passageways from the nasal cavity through the level of the terminal bronchioles (nose, pharynx, larynx, trachea, bronchi) (Sorokin, 1988). The respiratory portion of the lungs includes the small air

spaces from the respiratory bronchioles to the level of the alveoli (respiratory bronchioles, alveolar ducts, and alveoli) (Sorokin, 1988). The conducting portion functions to bring air in and out of the lungs, whereas the respiratory portion provides an outlet for gas exchange.

Gas exchange occurs through the thin walled structures, termed pulmonary alveoli. More than 300 million alveoli in the human lung provide at least 143 square meters of surface area for gas exchange between the inspired air and circulating blood (Sorokin, 1988).

The alveolar epithelium consists of two cell types, including the Type I and Type II alveolar cell. Type I alveolar cells cover a large surface area and are a specialized squamous epithelium that on average are less than 0.2 μm thick (Sorokin, 1988). Type I alveolar cells are the primary alveolar cells involved in gas exchange in conjunction with the endothelium of the alveolar capillaries (Apparao et al., 2010). Type I alveolar cells are connected to one another and to Type II alveolar cells by occluding junctions (Bloom and Fawcett, 1986).

Type II alveolar cells are located in the margins of alveoli and are classified as a cuboidal epithelium (Apparao et al., 2010). These secretory cells synthesize and secrete pulmonary surfactant, which is a phospholipid that coats the epithelial lining of the alveoli (Bloom and Fawcett, 1986). Type II cells are not primarily involved in gas exchange, but are structurally related to the organization of the blood-air barrier. Type II cells also support host defense in immune responses and act as epithelial progenitors (Apparao et al., 2010).

Together Type I and Type II alveolar cells comprise one side of the blood-air barrier; the opposite surface is made up of capillary endothelial cells. These capillaries, which bring blood to the blood-air barrier of the lung, are surrounded by the interstitium of the alveolar septa. Pulmonary epithelium overlies the capillaries at the points where gas exchange occurs - and in these areas, the interstitium of the lung is reduced to a thin layer of BM (Sorokin, 1988). Thus, oxygen exchange occurs through the blood-air barrier, beginning with the endothelium of the capillaries, followed by the BM of alveolar capillaries, the thin and sometimes indistinguishable interstitial space, the BM of the alveolar epithelium (type I cells), and finally the alveolar epithelium itself (Sorokin, 1988). The alveolar epithelial BM and endothelial BM of the capillary frequently are fused to form the PABM.

Pulmonary Alveolar Basement Membranes

The PABM in the lung is also referred to as the basement membrane zone (BMZ) (Evans et al., 2010). The terms basal lamina (BL), basement membrane zone (BMZ), and PABM are used interchangeably in the literature. Typically, BM is utilized more often in reference to the structure as it appears in light microscopy whereas BMZ and BL refer to the same structure at the electron microscopic level or when describing its molecular components. The BMZ (herein referred to as the PABM) is comprised of following three layers; the lamina lucida, lamina densa, and lamina reticularis (Evans et al., 2010).

On the basolateral surface of the alveolar cell, the lamina lucida (LL) forms the first layer of the PABM. This layer is comprised of collagen (XVII), laminin (5, 6, and 10), integrins ($\alpha 6\beta 4$), laminin (1), and collagen (IV) (Evans et al., 2010). The latter two proteins are found at the cellular-matrix interface of the LL (Evans et al., 2010). The

lamina densa is formed primarily by proteins such as entactin/nidogen, proteoglycans (perlecan, bamacan, agrin, collagen XVIII), and stored growth factors (FGF-2) (Evans et al., 2010). At the matrix interface, the lamina reticularis (LR) is comprised of the following molecular components: collagen (I, III, V, VI, and VII), proteoglycans (perlecan, bamacan, and collagen XVIII), as well as stored growth factors (FGF-2) (Evans et al., 2010).

In the lung, the lamina reticularis (LR) is the basal portion of the BM and has also been referred to as the reticular BM in the literature (Evans et al., 2010). The LR is variable in its distribution throughout the body and is not found in all tissues. However, it is present in a number of tissues with multilayered epithelium, including the lung (Evans et al., 2010). In pathological states, the LR is often affected, as it serves as a regulator of cytokine movement between the alveolar epithelium and the ECM (Evans et al., 2010). Interactions involving ECM macromolecules and the LR have the potential to alter cellular behavior. Diseased states can interrupt normal signaling cascades by altering cellular environments – such as the hyperglycemic environment generated by chronic DM.

Objectives of Current Study

Elucidating the molecular and cellular biological pathways contributing to the diseased microvasculature in DM is an important area of investigation. As previously stated, BM thickening is one of the hallmarks of microvascular complications in DM (Carlson et al., 2003). It is the first pathophysiological change in several tissues, including the glomerulus of the kidney, myocardial capillaries in the heart, as well as the capillaries of the retina (Liang, 2002, Carlson et al., 2003, 2012).

In this regard, the lung is the most highly vascularized organ in the body (Sorokin, 1988), and since DM is principally a disease of small blood vessels, it seems reasonable that the blood-air barrier is highly vulnerable to diabetic microangiopathy, (Shafiee et al., 2013) including PABM thickening.

Accordingly, my working hypothesis is that PABMs exhibit DM-related thickening in severely diabetic transgenic mice. Moreover, this structural alteration is mitigated by specific endothelial targeted overexpression of MT.

If my hypothesis is correct, the results will show that PABM are thicker in severely diabetic (OVE) mice than in the healthy control (FVB) and (Jtmt) groups. Furthermore, the bi-transgenic (OVEJtmt) group will show a reduced or even eliminated PABM thickness increase, strongly suggesting possible antioxidant protection against hyperglycemia-driven pulmonary oxidative stress.

Results of this study will contribute significant and fundamental data to the literature on diabetic BM disease. Furthermore and importantly, baseline ultrastructural data on the respiratory filtration barrier and a possible first definition of “diabetic pulmonopathy” and potential pulmonoprotection against vascular injury, will offer an avenue of new and compelling diabetes research.

CHAPTER II

MATERIALS AND METHODS

Research Animals

Four groups of mice were utilized in this study. Each group was further divided into two age cohorts including 60 and 150 day old mice. All groups consisted of at least 12 (six, 60 day-old and six, 150 day-old) animals. Group I was comprised of healthy control Friend virus B-type (FVB) mice (Taketo, 1991). Group II was age-matched, transgenic and severely diabetic mice (OVE) (Epstein et al., 1989, 1992). Group III consisted of at least 12 age-matched, transgenic (Jtmt) mice that overexpress metallothionein (MT) in endothelial cells (Teiken, 2011). Group IV consisted of at least 12 age-matched, bi-transgenic and severely diabetic (OVEJtmt) mice. The latter were derived from an OVE and Jtmt cross. All transgenic diabetic mice were easily identified by a phenotypic marker, which resulted in small eyes, by the intentional co-integration of the cataract inducing GR19 gene (Liang et al., 2002).

Before sacrifice, mice were weighed and tail tips snipped to procure blood samples utilized in hemoglobin A1c (HbA1c) and blood glucose analysis. Micromat II (Bio-Rad, Hercules, CA) kits were utilized for HbA1c measurements. The AlphaTRAK Blood Glucose Monitoring (test strips and glucose meter) System (Abbott Laboratories, Chicago, IL) was employed for blood glucose measurements.

All animals were kept in a controlled environment, on a 12-hour light and dark cycle, at the Biomedical Resources Facility at the University of North Dakota. Cages

contained natural pine and/or corncob bedding, which was changed routinely. Purina rodent laboratory chow and water were available to the mice at all times and animals were maintained according to standards set by the U.S. Department of Agriculture and the Institutional Animal Care Committee at the University of North Dakota.

Genotyping

The genetic strain of each mouse was confirmed by real-time polymerase chain reaction (RT-PCR), which identified the presence of the *MTII* transgene. The genetic strain identified diabetic and other transgenics from background or control mice. To extract DNA, approximately 0.5 cm of tail tips were snipped (with sterilized scissors, washed in 70% EtOH between each sample) and immersed in 100µl of Extraction Solution (Sigma-Aldrich REDEExtract-N-Amp Tissue PCR Kit, Cat. #E7526) in a sterile 500 µl microcentrifuge tube. Twenty-five microliters of Tissue Preparation Solution was added to each microcentrifuge tube and vortexed thoroughly. Tissue digestion was carried out by placing the samples in a 55°C incubator for ten minutes, followed by a three-minute incubation in a 95°C water bath. One hundred microliters of Neutralization Solution B was added to the samples followed by vortexing. The neutralized tissue extract was then stored at 4°C until further PCR amplification.

PCR Amplification

To determine the genetic strain of the research animals, PCR amplification was performed. According to vendor (Sigma-Aldrich) instructions, DNA was extracted from tail tissue using the REDEExtract-N-Amp PCR Reaction Mix (Sigma-Aldrich, Cat. #R4775) as described above. For each sample, 10 µl of REDEExtract-N-Amp PCR Reaction Mix, forward and reverse primers (50 nmol/ml), and dH₂O were brought to a

final volume of 16 µl. Forward and reverse primers (Invitrogen) targeted the human *MTII* gene that was inserted in the *Jtmt* transgene as described previously (Teiken, 2011). The *MTII* forward primer (AATCGGTTGTGGACTGAGGA) and reverse primer (TCACGGTCAGGGTTGTACAT) generated a 536 bp product and control (FVB) strains with the forward primer (TCACAATCACCAGGTTTCCAA) and reverse primer (CAGCCCAGTCAGAAGTCTAAA) generated a 200 bp product (Teiken, 2011).

In a sterile 200 µl microcentrifuge tube, 4 µl of DNA and 16 µl of PCR Reaction Mix were combined, vortexed, and were then subjected to PCR thermal cycling. The cycling parameters used were as follows: initial denaturation at 94°C for three minutes (one cycle), denaturation at 94°C for one minute, annealing from 45 to 68°C for one minute, and reverse priming at 72°C for one-two minutes (all three previously described steps repeated for 30 cycles), and finally tissue extraction at 72°C for one cycle of ten minutes. Then samples were loaded directly onto a 1% agarose gel.

Agarose Gel Electrophoresis

Following PCR amplification, 10 µl of amplified DNA was loaded directly into 1% agarose gels. Gels were prepared by adding 0.5 g of agarose (Fischer) to 50 ml of 1xTAE buffer (BIO-RAD), heated at power level 10 for 60 seconds in a General Electric Turntable Microwave Oven, and gently swirled until all the agarose dissolved. The solution was cooled for a minute, after which 3.5 µl of 10 mg/ml ethidium bromide (ETBR) was added. The gel was poured into a casting platform and allowed to set for at least 20 minutes before samples were added to the wells (formed from the comb inserts that were placed into the gel during the cooling and solidifying stage). Finally, 1x TAE buffer was poured onto the gel and 10 µl of the samples were added to each well. The

samples were run at 80 volts for 40 minutes subjacent to a DNA molecular weight marker. Gels were viewed using a High Performance Ultraviolet Transilluminator (UVP –Ultraviolet Products). To process and document images, a Carestream GEL Logic 112 Imaging System was employed.

Quantification of MT in Pulmonary Tissues

Tissue Preparation.

At 110-170 days of age, FVB, Jtmt, OVE and OVEJtmt, animals were deeply anesthetized by injection of sodium pentobarbital (50 mg/ml, 100 mg/kg body weight). Upon the absence of limb withdrawal and corneal reflex responses, the abdominal and thoracic cavities were quickly incised and the right atrium cut to allow for exsanguination and fluid drainage. Pulmonary tissues were harvested, rinsed in saline, blotted dry, and weighed. The tissues were then immediately frozen in liquid nitrogen before storage at -80°C. Tissues were thawed and minced with a razor blade before placing in ultracentrifuge tubes with 2 ml cold (4°C) 0.1M Tris buffer (pH 10.4). For each mouse (except the OVE for which only one lung was taken), both lungs were placed in one ultracentrifuge tube. Tissues were sonically disrupted using a Sonic Dismembrator (Fisher Scientific) until completely in solution. The tissue suspensions were centrifuged at 30,000 rpm for 1 hour at 4°C. Supernatants from each sample were collected, vortexed, aliquoted into 4, 1.5 ml centrifuge tubes and stored at -80°C.

Bradford Assay

The Bradford assay (Bradford, 1976) was used to quantify the amount of total protein in lungs from all mouse genotypes. For each assay, a standard curve was generated from a bovine serum albumin (BSA) solution (10 mg/ml; Sigma) diluted in

0.01M PBS (Sigma) to a range of 120 µg/ml to 5 µg/ml. PBS was used as a blank. Tissue supernatants were diluted in PBS 1:100, 1:200 and 50 µl of each standard and sample solution was loaded onto clear polystyrene 96-well plates (Fisher). Bradford reagent (Bio-Rad) was diluted 1 part reagent to 4 parts dH₂O and 150 µl was added to each well. Color development was read on a SPECTRAmax PLUS microplate spectrophotometer (Molecular Devices) at a wavelength of 590 nm and the data analyzed by SOFTMax software.

MT Competitive ELISA Assay

A competitive ELISA developed by Drs. John Swinscoe and Mandy Meyer (Meyer, 2006) was used to quantify the MT in pulmonary tissues from FVB, Jtmt, OVE and OVEJtmt mice. For each assay, a Costar EIA/RIA 96-well polystyrene plate (Fisher) was coated with 50 ng of MTII protein (rabbit liver; Axxora) in 100 µl of 0.1M Tris (pH 10.4) per well and wells that would serve as blanks received only 0.1M Tris. The plate was incubated for 6 hrs at room temperature 4°C with slow rotation then washed 3 times with wash buffer (0.01M Tris, 0.02 NaCl, 0.1% Tween 20, pH 7.2). Standard MTII (1 µg; rabbit liver; Axxora) was polymerized in 3% glutaraldehyde, and 5 µl 0.1M Tris and the tissue sample supernatants were also polymerized in 3% glutaraldehyde on ice for 60-90 min. Metallothionein readings were maximized at 90 min. A primary antibody solution was made by diluting the monoclonal mouse anti-horse MTI/II antibody (Dako, Carpinteria) 130 mg/L; Invitrogen) 1:1000 in primary antibody buffer (0.1M Tris, 0.1% Tween 20, pH 10.4) and kept on ice until use.

After the 90 min incubation on ice, the standard MTII polymerized solution was diluted to 400µl with 0.1M Tris. A standard curve ranging from 0-10 ng of MTII was

generated using 16, 12, 8, 4 μ l of this standard MTII solution added to 400 μ l of the primary antibody solution. The polymerized sample supernatants were also added to 400 μ l of the primary antibody solution at room temperature.

The plate was washed 3 times in wash buffer. Then 100 μ l aliquots of standard or sample solution were added to 4 wells. Half of the blank wells received 100 μ l of 0.1M Tris and the remaining half received 100 μ l of primary antibody buffer. The plate was incubated at 4°C overnight.

The plate was washed in wash buffer 3 times. Then, each well received 100 μ l of alkaline phosphatase conjugated anti-mouse IgG (1:2500 in 0.01M sodium phosphate, 0.02M NaCl, 0.1% Tween 20, pH 7.2; Sigma) and the plate was incubated at room temperature for 2 hours. The plate was again washed 3 times with wash buffer followed by a final wash with dH₂O. Color was developed by the addition of 4-nitrophenyl phosphate disodium salt (10 mg in 10% diethanolamine, pH 10; Sigma). Color was allowed to develop for 20-30 minutes. The plate was read on a SPECTRAmax PLUS microplate spectrophotometer (Molecular Devices) at a wavelength of 405 nm, and the data analyzed by SOFTMax software.

Metallothionein values were divided by the volume of tissue sample per well to generate a value as ng/ μ l that was then adjusted to μ g/ml. This value was divided by the appropriate sample Bradford protein data (μ g/ml) to yield the final amount of MT per sample as μ g/mg pulmonary tissue protein.

Vascular Perfusion and Tissue Preparation for Microtomy

In an effort to prepare excellent samples for immunohistochemical (IHC) or morphometric analysis, animals were sacrificed by vascular perfusion through the left

ventricle. Prior to perfusion, mice were anesthetized by intraperitoneal (IP) injection of sodium pentobarbital (100 mg/kg). Limb and eye reflexes to sensory stimulation were checked prior to any incisions, ensuring that the animals were deeply anesthetized. Micro-surgical scissors were used to incise the right atrium, to allow fluid drainage and exsanguination. Immediately following the incision, a 26G 3/8" hypodermic needle (B-D & Co., Rutherford, NJ), attached to plastic medical grade 0.020 inch tubing was inserted into the left ventricle for infusion of 50 ml warm isotonic (0.9M) saline and additional perfusates to clear the vascular bed. Flow rates for saline and fixatives were set at approximately 6 ml/min. At the time of perfusion, several organs including the lung, heart, kidneys, and retinas were harvested to prepare an adequate diversity of tissue sample. Perfusion was deemed adequate when eyes, lips, and tail of the mouse became pale and limbs were rigid.

Perfusion Using Zamboni's Fixative

Tissue samples prepared for IHC analysis were perfused and fixed with Zamboni's (Zamboni and Stefanini, 1968) fixative. This fluid was prepared by dissolving 4 g of paraformaldehyde in 25 ml of distilled water heated to 50°C. Twenty ml of 0.5M sodium phosphate buffer and 16.5 ml picric acid were added to the solution, which was then stirred, cooled to room temperature, and filtered. The solution was brought to a final pH of 7.4 by drop wise addition of 1N sodium hydroxide (NaOH) or 1N hydrochloric acid (HCl). The fixative was brought to a total volume 100 ml by adding 38.5 mL of dH₂O.

Prior to perfusion, animals were anesthetized as described above. Perfusion was initiated with 50 mls of filtered prefixative (0.9% NaCl, 0.1% NaNO₂, and 100 units of

heparin in dH₂O) administered at a rate of 6-7 ml/min, followed by 100 mls of full strength Zamboni's fixative. Immediately following perfusion, pulmonary tissue was surgically removed and immersed in cold Zamboni's fixative for three hours. Tissues were stored in 25% sucrose buffer (sucrose, glycerol, 0.5M phosphate buffer, 1% sodium azide in dH₂O) at 4°C overnight before embedding in paraffin.

Perfusion Using PIPES Fixative

All animals were adequately anesthetized and perfusion was initiated as previously described. For preparation of tissue samples for TEM observation and TEM morphometry, glutaraldehyde-based PIPES fixative (Bauer and Stacey, 1977) was employed. PIPES fixative was freshly prepared for each perfusion procedure. The fixative consisted of PIPES buffer (PIPES {Piperazine-N,N'-bis[2-ethanesulfonic acid]} (Sigma: P8203-250G), 1N NaOH, distilled water), and 20% dextran (Sigma: D4626), 10% paraformaldehyde, and TEM grade glutaraldehyde 10% (Tousimis, #1060A). Following observation of clear fluid drainage from the right atrium, 20 ml of warm fixative and then 40 ml of cold fixative was administered. Organs harvested from mice were immediately immersed in vials of cold PIPES fixative for approximately 30 minutes.

Tissues were minced to 1 mm³ blocks and placed in cold fixative for three hours and then washed in PIPES buffer with 2% sucrose for 30 minutes, at room temperature. Blocks were then immersed in a 1:1 solution of 2% osmium (OsO₄) (Stevens Metallurgical Corp., NY, NY), 3% potassium ferricyanide (K₃Fe(CN)₆ and distilled water in PIPES buffer with one part PIPES buffer, 6% (sodium iodate) NaIO₃ (Fisher Cat # 5322-100 P.259C) and 4% sucrose overnight. Following overnight treatment with

buffered OsO₄, tissue samples were dehydrated in an ascending series of alcohols as follows: two five-minute treatments with 15% ethanol (EtOH), two ten-minute treatments with 30% EtOH, two 15 minute treatments with 50% and 70% EtOH, three 20-minute treatments with absolute EtOH, and finally, two one-hour washes in absolute EtOH.

Following dehydration, tissues were rinsed briefly in propylene oxide (1,2 epoxy propane), followed by two additional 15-minute propylene oxide washes, and a 1:1 solution of epoxy resin and propylene oxide. The epoxy resin consisted of Araldite 502 – Modified Bisphenol A Epoxy (EMS, Cat. #10900), EMbed-812 (Epon-812 Substitute) (EMS, Cat. #14900), Dodecenyl Succinic Anhydride (DDSA) (EMS, Cat. #13710), and 2,4,6,-{Tri(Dimethylaminoethylphenol)} (DMP-30) (EMS, Cat. #13600).

The final step in tissue preparation included an overnight incubation in a 3:1 solution of epoxy resin and propylene oxide before an 18-hour incubation in full strength epoxy resin. All tissues were then embedded in fresh epoxy resin and incubated at 65°C for at least 72 hours.

Paraffin Embedding

Tissues perfused with Zamboni's fixative were embedded in paraffin for immunohistochemical analysis by light microscopy. Tissue dehydration was carried out in a series of graded alcohols, beginning with 50% EtOH for 30 minutes, followed by 70%, 80%, 95%, and 100% EtOH for 30 minutes each (repeated twice). Tissues were then immersed in two washes of CitroSolv (Fisher) for 20 and 30 minutes followed by 60 minutes in a 1:1 Paraplast (Fisher):CitroSolv solution, and two 60-minute rounds in full-strength Paraplast in a vacuum oven at 60°C. Pulmonary tissue was embedded in

plastic molds using a cooling table on a paraffin embedding apparatus. Tissues were maintained at -20°C for at least 24 hours prior to sectioning.

Immunohistochemistry

For IHC analysis, paraffin blocks were trimmed with tEM single-edge stainless razor blades (Tousimis #7250) to form a pyramidal shape face. Blocks were then placed in a Leica RM2125 microtome and sections of tissue were cut at approximately 5-7 µm with a biological grade steel knife. Ribbons of tissue serial sections were placed in a water bath (40°C TissuePrep). Sections were collected on glass slides coated with poly L-lysine (Histology Control Systems, Glen Head, NY). Slides were stored at 4°C until they were used for IHC procedures.

A Tissue-Tek® Slide Staining Set (Electron Microscopy Services) was used to immerse slides in CitroSolv for paraffin removal. This was repeated three times for five minutes per immersion, followed by subsequent rehydration in a series of graded alcohols (70%, 95%, and 100% EtOH three times for 5 minutes). Slides were then rinsed for five minutes in gently running cold tap water. A liquid blocker PAP-pen (EMS, Cat. #71310) was used to encircle the tissue on slides after the five-minute water bath, and the slides were placed in a humidifying chamber with 3% hydrogen peroxide (H₂O₂) for one hour. Next, slides were subjected to 10% normal rabbit serum for 20 minutes and then mouse-to-mouse blocking reagent (Scytek) for 30 minutes. After a one-hour incubation in 1% Blocking Reagent (Invitrogen) [10mg/ml in 0.01M PBS (Sigma)], slides incubated for one hour in primary antibody, at a 1:100 dilution (in 1% Blocking Reagent). The MT primary antibody (mouse anti-horse MTI/II, Dako) was administered to positive controls (renal tissues from animals overexpressing endothelial MT (Teiken, 2011)), while the

same tissue treated with 1% Blocking Reagent only served as negative controls. Slides were then rinsed three times in 0.01M PBS, then treated one hour with biotinylated rabbit anti-mouse IgG (Invitrogen) at a 1:200 dilution in 1% Blocking Reagent.

Following three rinses in 0.01M PBS, slides were treated in a humidifying chamber with Horse Radish Peroxidase (HRP) conjugated streptavidin (Invitrogen) at a dilution of 1:500 in 1% Blocking Reagent. All slides were then exposed to a 1:10 solution of 3,3'-Diaminobenzidine (DAB) in 0.01M PBS and a 1:1000 solution of 30% H₂O₂. A final rinse in cold tap water preceded a nuclear counter stain with 0.5% methyl green on low heat. Slides were allowed to dry overnight prior to the addition of Permount attached cover slips and observed by bright field light microscopy.

Microtomy

Epoxy blocks containing pulmonary tissue were trimmed to form a trapezoid face with a 1 mm base with tEM single-edge stainless razor blades. An MTX ultramicrotome equipped with a gem grade diamond knife (DiATOME) and an MTX ultramicrotome was utilized for making thick and thin tissue sections. First, thick sections (250 nm) of tissue were made and examined by light microscopy to identify tissue location and position. Thick tissue sections were collected on a drop of dH₂O on a glass slide and were dried on low heat. Slides were stained with 1% toluidine blue in 1% sodium borate, and following the addition of cover slips were examined by bright field (Olympus BH-2) microscopy.

When ultramicrotomy was deemed appropriate, thin sections (70 nm) were cut and ribbons of tissue sections were collected in a dH₂O metal trough. A cotton swab dipped in chloroform was passed over the sections to eliminate wrinkles within the tissue.

Ribbons of tissue, with an optimal interference color of silver, were collected on 300 μm mesh naked copper grids.

Light microscopy

Glass slides stained with 1% toluidine blue or immunohistochemically, as described above, were viewed on a brightfield Olympus BHS (BH-2) light microscope. An Olympus 63x and 100x oil immersion objective lenses were used to view any pathological features of pulmonary tissue. Images were captured using a SPOT Idea Digital Microscope Camera and SPOT imaging software version 4.6 (Diagnostic Instruments, Inc.).

Staining procedure for TEM grids

Tissue samples for TEM on copper grids were stained with 2% uranyl acetate and lead citrate (Venable and Coggeshall, 1965). Uranyl acetate was prepared by dissolving 0.4 grams of uranyl acetate in 10 ml of distilled water. A one to one solution of 4% uranyl acetate was made with absolute EtOH, followed by filtration through a 0.2 μm filter (Thermo Scientific, Cat. No. 190-2520). Grids were stained for five minutes on silicone mats (PELCO®, #10521) in petri dishes covered with aluminum foil for protection from photon exposure. Grids were rinsed with distilled water before staining with lead citrate. Initially, 0.6 grams of lead citrate was mixed in 20 mls of boiled water, followed by the drop-wise addition of 10N sodium hydroxide to clear the solution (Venable and Coggeshall, 1965). The lead solution was then centrifuged for 15 minutes. The staining procedure was repeated, leaving grids on the silicone mats for 5 minutes in covered petri dishes lined with NaOH pellets to protect grids from CO₂ exposure. Grids

were then rinsed thoroughly in distilled water and allowed to dry for a minimum of 24 hours in grid storage boxes.

Transmission Electron Microscopy

Thin sections of pulmonary tissues were photographed in a Hitachi 7500 TEM at an initial magnification of x30,000. Ten micrographs were obtained from each tissue block (two blocks per mouse), totaling at least 240 micrographs for each mouse genotype. Micrographic films (Kodak 4489) were developed by conventional methods, scanned (Epson Perfection V750 Pro scanner), and printed (HP LaserJet P2015 printer) on plain 8.5"x11" paper. Prior to printing, each micrograph was magnified by exactly 2.8X (Adobe Photoshop) to guarantee a final magnification of precisely x84,000. This relatively high magnification was chosen to ensure accurate marking of PABMs on finished prints.

Random perpendicular widths of the PABM were marked utilizing a transparent grid overlay (three cm squares) placed onto each micrograph. This established true randomization in marking PABMs. Only points of PABM that intersected the grid were marked for measurement. Accordingly, all points along the PABM were equally likely to be selected and operator choice was not an option.

Unbiased TEM Morphometry

As mentioned above, operator bias in PABM measurement was eliminated and measurement consistency was maintained with the use of a transparent grid overlay. In pulmonary tissue, the inner plasma membrane of the endothelial cell (of the blood-air barrier) was used as a reference for the starting point of measurements. Where alveolar cells crossed the superimposed grid, a mark is made at the point of PABM intersection.

By the orthogonal intercept method (Jensen et al., 1979), a diagonal line was drawn across the PABM from the beginning reference point on the endothelial cell to the plasma membrane of the perpendicularly located alveolar cell. Using a digitizing tablet and specialized software (Bioquant, R and M Biometrics, Inc.), the length of the perpendicular lines (orthogonal intercepts) were measured and distributed into one of nine classes of thickness (Hirose et al., 1982). The harmonic mean apparent thickness (Dische, 1992) of the measurements was then calculated and multiplied by $8/3\pi$ (Jensen et al., 1979) to eliminate an expected right-sided skew of the numerical distribution and to give the true PABM width (Gundersen and Osterby, 1973).

At least ten images were taken of each block, which allowed for the analysis of at least 120 micrographs per mouse. On average, one micrograph provided approximately ten PABM measurements. Taken together, this resulted in > 485 micrographs measured in the 60 day-old group, and approximately 4,000 PABM measurements available to calculate harmonic means (Table 3). The 150 day-old cohort showed similar averages for blocks per mouse, micrographs obtained per block, and average number of PABM measurements per micrograph. Accordingly, the total number of PABM measurements used to calculate the harmonic means in the 150 day-old group was ~4,400.

Statistics

Distributions of “true” PABM thickness [as derived from orthogonal intercepts on sets of at least 20 micrographs for each animal type (FVB, Jtmt, OVE and OVEJtmt)] were statistically compared using the nonparametric Wilcoxon-Mann-Whitney rank-sum test as previously described (Carlson et al., 2003, 2004). Significance value for all tests was set at $P \leq 0.05$.

CHAPTER III

RESULTS

General Condition of Animals

In general, 60 day-old FVB and Jtmt mice are physically active, exhibit sleek and shiny coats, and are approximately of equal size (Figure 1A). The diabetic animals (OVE and OVEJtmt mice) also demonstrate active behaviors at 60 days. However, their coats are noticeably less sleek and appear patchy. All diabetics, including OVE and OVEJtmt mice are recognizable by their small eyes (Figure 1B), but otherwise cannot be distinguished from each other. No other obvious physical characteristics are different among the four genotypes.

Likewise, at 150 days of age, FVB and Jtmt mice are physically indistinguishable and maintain healthy body weights, sleek coats, and active physical dispositions. However, their diabetic counterparts are easily identifiable as they not only exhibit small eyes, but their coats are generally patchier and dull. Diabetic mice also tend to be somewhat lethargic and weigh less than Jtmt mice (Table 2). Glycated hemoglobin levels in OVE and OVEJtmt mice are consistently higher than FVB and Jtmt mice (Table 2). Fasting blood glucose measurements are consistent with HbA1c data and also are decidedly higher in the diabetics than FVB and Jtmt mice (Table 2).

Pulmonary Morphology

Light Microscopy

Light microscopic images of toluidine blue stained thick sections of pulmonary tissue from 150 day-old mice (Figure 2A) show typical textbook features of respiratory tissue. By this technique the terminal portion of the respiratory system can be visualized. This region contains terminal bronchioles, respiratory bronchioles, alveolar ducts, alveolar sacs, and individual alveoli. However, only alveolar ducts, alveolar sacs, and alveoli are seen by conventional toluidine blue staining (Figure 2A). Alveolar ducts are surrounded by pockets of alveolar sacs that terminate in individual alveoli. The latter are separated from each another by alveolar septa. Small veins also can be seen in cross section, with occasional intravascular erythrocytes. Individual components of alveolar walls cannot be identified at the LM level, but the thin respiratory filtration barrier can still be appreciated. Type I alveolar cells are the most common cell type contributing to the large surface area for gaseous exchange. This extensive layer is manifested morphologically as an external attenuated cytoplasm of the respiratory filtration barrier.

Transmission Electron Microscopy

Components of the respiratory tissue in 150 day-old FVB mice that are not identifiable at the LM level, are clearly resolved by TEM. The small rectangular area drawn in the large original LM image (Figure 2A) illustrates the approximate size of the area shown in the TEM inset at the bottom of the figure (Figure 2B). The inset TEM image (Figure 2B) illustrates structures that could be expected to be found included in the small rectangle in Figure 2A at an original magnification of approximately 100x. Type II alveolar cells are located in the inter-alveolar septa where they offer structural support to

surrounding alveolar and capillary networks. Circulating lymphocytes and erythrocytes occasionally occupy capillary spaces. Structural components of the respiratory filtration barrier, such as the meshwork of elastin and collagen that lies within the extracellular space, can usually be found in the alveolar septa. Intracellular structures in type II alveolar cells (e.g. nuclei and lysosomes) can be identified by low magnification TEM (Figure 2B).

Increasing the TEM magnification to 16,000 diameters offers a sharper resolution and the PABM appears as an electron dense structure surrounding alveoli, though the PABM still is not easily measured for data collection and analysis (Figure 3). Bundles of elastin are also more apparent at this magnification. They are often located in the structural matrix between A1 and A2 cells, (located in the upper right corner of the Figure 3). Endothelial cells line the capillary space and are present on the intravascular side of the PABM. Alveolar type I cells line the air space on the opposite side of the PABM. Other interesting features include endothelial flaps that are identifiable where endothelial cells come together to form tight junctions.

Increasing to an even higher magnification of 60,000 diameters (Figure 4) demonstrates individual components of the respiratory filtration barrier and allows for consistent, accurate, and unbiased PABM measurement and data collection. The cytoplasm of the thin endothelial cells line the internal side of the blood-air barrier, and is separated from the alveolar epithelium by the PABM. Endothelial cells are orientated toward the left and right external side of the filtration barriers in Figure 4. Type I alveolar cells line the air space and are located toward the middle of the micrograph. Between the

two cell layers, the PABM runs the length of the micrograph in a superior to inferior direction.

At the LM level, individual PABMs are not recognizable or measureable. Accordingly, in the current study TEM is required to clearly and reliably identify the limits of the PABM of the lung. Four groups of mice are utilized to study the PABM, and at 60 days of age, and a magnification of 60,000 diameters, variations in PABM thickness between genotypes can be appreciated (Figure 5). The PABM of each mouse genotype is illustrated by the opposing arrowheads and are ordered as follows; 60 day-old FVB PABM (Figure 5A), 60 day-old Jtmt PABM (Figure 5B), 60 day-old OVE PABM (Figure 5C), and 60 day-old OVEJtmt PABM (Figure 5D). In Figures 5 A-D, endothelial cells are much thinner than type I alveolar cells. This structural characteristic is an excellent aid in discriminating between capillary and alveolar components of the respiratory filtration barrier. Endothelial cells in each image in Figure 5 are positioned toward the superior portion of the micrograph (as indicated in Figure 5D), and the A1 cells face the inferior portion of the PABMs in Figures 5 A-D. Generally, the capillary endothelium lines the concave side of the PABM and type I alveolar cells form its convex border.

Micrographs of 150 day-old lung tissue show morphological features remarkably similar to those obtained at 60 days of age. By visual inspection, the PABM of 150 day-old FVB mice (Figure 6A) appears considerably thinner than PABMs from Jtmt (Figure 6B), OVE (Figure 6C), and OVEJtmt (Figure 6D). Significantly, the 150 day-old OVE (Figure 6C) PABM is appreciably thicker than the other age-matched PABMs in Figure 6. Similar to observations in the 60 day-old lungs, the endothelial cells are much

thinner compared to their type I alveolar cell counterparts, and are orientated in the same manner as previously described.

Pulmonary Alveolar Basement Membrane (PABM) Morphometry

Interestingly, PABM measurements obtained in the 60-day group generate harmonic means within a very small range (Figure 7) shown as the PABM thickness of FVB, Jtmt, and OVE mice all approach 50.0 nm. These data affirm our preliminary visual observations of these PABMs, which suggest that they are relatively similar in width. Statistical significance value is set at $P < 0.05$.

As anticipated, the greater PABM thickness differences noted by preliminary visual observation in 150 day-old mice relative to 60 day-old animals is confirmed by orthogonal intercept analysis (Figure 8). Not surprisingly, the OVE genotype exhibited the thickest PABM measurements. Moreover, the largest margin of difference between any two genotypes was the interval between 150 day-old OVE and OVEJtmt mice. The nonparametric Wilcoxon-Mann-Whitney rank-sum test indicated statistical significance between PABM thicknesses in the FVB and OVE groups ($P = 0.020$), Jtmt and OVEJtmt groups ($P = 0.0095$), and OVE and OVEJtmt groups ($P = 0.012$) at 150 days of age. Statistical significance value is set at $P < 0.05$.

When both age groups are analyzed together, statistically significant differences were observed between the 60 day-old OVE and 150 day-old OVE genotypes (Figure 9). However, this significant difference is completely eliminated when OVEJtmt mice in the two age groups are compared. Interestingly, FVB mice show no significant changes in PABM width with age. (Figure 9). Significantly, 150 day-old Jtmt PABMs average ~52.76 nm, a 5.4% thickness increase over 60 day-old mice of the same group. At 150

days, PABMs in OVEJtmt mice are increased by 6.1% over 60 day-old mice (~47.75 nm compared to ~44.97 nm) while OVE mice show the largest age-related PABM width increase, an average of ~51.49 nm compared to ~58.42 nm, or approximately 18.3%.

When compared to age matched controls, 150 day-old mice exhibit diabetes-induced PABM thickening in the OVE group (~58.42 nm) but more importantly; a significantly ($P = 0.012$) reduced PABM width is demonstrated in OVEJtmt mice (~47.75 nm). Also, FVB mice show levels of thickening similar to the Jtmt group with averages of ~48.71 nm and ~52.76 nm, respectively (Figure 9A).

Analysis of MTI/II Expression

Immunohistochemical Analysis of MTI/II in 150-Day Lung Tissue.

To identify the expression of MT I/II in endothelial cells of the lung, IHC analysis was utilized. Positive controls from Jtmt mice were obtained from the kidney (Figure 10B) and were treated with primary antibody as previously described. Negative controls were derived from the same tissue. However, these samples were not exposed to primary antibody and received blocking reagent in its place. As expected, the positive controls showed light brown staining of the MT I/II antibody in the endothelium. Negative controls indicated no MT I/II staining.

Positive staining for MT I/II in the endothelium of the lung was also visible (Figure 10D and F). Lungs from Jtmt and OVEJtmt showed positive expression of MT I/II as indicated by light brown staining around the endothelium of small veins. Immunohistochemical staining indicated that MT I/II was expressed in the pulmonary vasculature of the transgenic mouse lines, which suggested quantification of MT I/II could be executed.

Competitive ELISA of MTI/II in 150-Day Lung Tissue

At 150 days of age, lungs from an FVB, OVE, Jtmt, and OVEJtmt mouse were obtained to quantify MT I/II present in pulmonary tissue by the competitive ELISA method. Metallothionein levels were expressed per total μg of protein in each tissue sample. Levels of MT I/II in each genotype were as follows: FVB (0.23 $\mu\text{g}/\text{mg}$), OVE (0.22 $\mu\text{g}/\text{mg}$), Jtmt (0.45 $\mu\text{g}/\text{mg}$), and OVEJtmt (0.33 $\mu\text{g}/\text{mg}$). Importantly, the Jtmt lung measured MT I/II two times the amount found in the FVB control. The OVEJtmt pulmonary tissue also measured higher MT I/II protein levels than the controls, but were not as elevated to the levels of the Jtmt pulmonary tissue. Data obtained from this method was remarkably consistent with the staining patterns found in IHC analyses of the same tissue.

CHAPTER IV

DISCUSSION

Basement membrane thickening was identified in diabetic patients more than 50 years ago and has long been considered the morphological hallmark of the disease (Bergstrand and Bucht, 1959). Early studies on the effects of DM on BMs indicated changes in protein composition in diabetic mice compared to healthy controls (Rohrbach and Martin, 1982). Laminin and collagen IV synthesis was induced in diabetic mice, although the synthesis of proteoglycans was inhibited in these same animals. Treating diabetic mice with insulin returned the synthesis of proteoglycans to normal levels over time, suggesting that the lack of heparan sulfate proteoglycan stimulated the overproduction of laminin and collagen IV in an effort by cells to compensate for the loss of proteoglycan synthesis leading to decreased BM turnover and increased BM width (Rohrbach and Martin, 1982).

More recent studies on diabetic animals have suggested that although expression of some ECM proteins is increased, it is not clear that such synthesis is the result of compensatory hypertrophy. In fact, it is apparent that BM thickening in most diabetic models is due largely to the lack of breakdown and turnover of matricellular molecules, and not an overexpression of various ECM proteins (Tsilibary, 2003).

Although the mechanisms leading to increased BM width have been elusive, as pointed out in the Introduction, considerable progress has been made in unpacking the

potential regulatory pathways leading to decreased ECM turnover in DM. Recently, an interesting unifying hypothesis was offered (Brownlee, 2001) that suggested that in the hyperglycemic state, oxidative stress, mainly derived from mitochondrial activity, generated high levels of free radicals (small charged oxygen ions), capable of considerable tissue damage. Moreover, numerous studies aimed at reducing the mass of free radicals have reported remarkable mitigation of a variety of chronic diabetic complications in the kidney and heart, (Carlson et al., 2013; Velic et al., 2013).

A review of the literature shows that attempts to link DM and pulmonary structure and function have been sparse, inconsistent and contradictory. Basement membrane thickening in the lung has been reported in several pulmonary pathologies, but has not been correlated directly with DM. Typically BM thickening has been identified in other diseases, including asthma, chronic obstructive pulmonary disease, tuberculosis, and lung cancer (Watanabe, 1997). However, BM thickening in these studies focused primarily on bronchiolar BMs and cannot be compared to PABMs, where the majority of gas exchange occurs.

It must also be pointed out that diabetes-related research has not focused on pulmonary tissues because of the high probability that extant clinical complications may be masked by more serious manifestations, including kidney failure. Nevertheless, a few studies (Vracko, '79; Kida et al., '83; Fuso et al., '96) have given some attention to the diabetic lung and suggest that pulmonary tissues may be somewhat affected by the disease.

In 1979, Vracko utilized post mortem tissue from human diabetics in a TEM analysis of alveolar and pulmonary capillary basement membrane thickening of diabetic

patients. Unfortunately, the PABM thickening data was not measured at the points where alveolar and endothelial BMs fuse to form the PABM. Additionally, the data was not correlated with the duration of the disease, or with the age of the patient.

A later study (Kida et al., 1983) centered on the volume proportion of the alveolar wall, reported a 24% increase in streptozotocin-induced diabetic rats, though the data was not statistically significant. On the other hand, these investigators demonstrated a significant increase in the number of alveoli (per unit volume) in diabetic rats compared to normal controls, as well as an increase in surface to volume ratio (Kida et al., 1983). However, a direct correlation between DM and these changes could not be shown because the effect of insulin treatment was not studied. Accordingly, potential side effects of streptozotocin (a nephrotoxin and possible pulmonotoxin) on the lung could not be ignored (Ofulue et al., 1988).

Furthermore, it has been speculated that diabetic patients, specifically Type I diabetics, have a decreased capillary blood volume and carbon monoxide diffusing capacity (Fuso et al., 1996). However, published results on this subject are conflicting (Fuso et al., 1996). Contradictory data reported in studies measuring diffusing capacity and capillary blood volume, were likely due to differences in the manner in which patients were tested (e.g. supine vs. sitting). It is well known that variations in testing parameters (including body position in pulmonary function tests) alters the functional recruitment of superior pulmonary lobe capillaries as well as the specificity and sensitivity of these tests (Fuso et al., 1996).

Accurate histological descriptions of pulmonary alveoli demonstrate a three-layered structure including an external layer of alveolar cells, and an internal layer of

endothelial cells both of which lie immediately subjacent to the central PABM (Cross and Mercer, 1993). In vertebrate animals, this tripartite morphological pattern is repeated only in the urinary filtration barrier of the kidney where the GBM is lined internally by glomerular podocytes and externally by fenestrated endothelium. To be complete, the choroid plexuses located in the ventricles of the brain exhibit some structural similarities but only in the lung and kidney are two BMs truly fused to form a single PABM or GBM that serves as a passive (though size-selective and charge-selective) filter.

Despite patient compliance and rigid insulin injection schedules, increased GBM width is widely recognized as a diagnostic feature of both Type I and Type II DM. Interestingly, its pulmonary counterpart is rarely mentioned and has received little morphometric investigatory activity.

Accordingly, the current investigation was designed to follow up on a single preliminary study by Carlson et al., (2003) that showed that although not all varieties of BMs are subject to significant diabetic thickening, the GBM and several other types, including PABM, were remarkably vulnerable to thickening in severely diabetic OVE mice.

The present study was patterned after a remarkable investigation (Zheng et al., 2008) that reported severely diabetic (OVE) mice were protected against albuminuria and several other diabetic parameters by crossing them with transgenic mice with specifically targeted antioxidants (MT), particularly powerful scavengers of free radicals injurious ions widely suspected to mediate tissue damage in most chronic complications of DM. In fact, the ROS scavenging activity of MT has been shown to be greater than 50 times more effective than GSH (Sato and Bremner, 1993).

These studies motivated co-workers in the Carlson laboratory (University of North Dakota School of Medicine and Health Sciences) to investigate the efficacy of MT in ameliorating diabetic complications, including BM thickening, in the heart (Velic et al., 2013), kidney (Carlson et al., 2013), and pancreas utilizing unbiased TEM morphometry (Chen et al., 2001). The results of these studies were universally positive and in each case, breeding OVE diabetic animals to specific MT overexpressors (Nmt, glomerular podocytes; MT, cardiomyocytes), BMs of subjacent microvascular cells in the diabetic animals were significantly protected from reaching the widths of untreated diabetic mice.

These results concerted efforts to generate a strain of mice in which the effect of MT overexpression could be evaluated more globally. Therefore in 2011, Teiken utilized the *Tie2* promoter and the MT II isoform to generate a plasmid that could be used to develop a transgenic mouse that overexpressed MT specifically and ubiquitously in endothelial cells.

Importantly, immunohistochemical analysis confirmed that MT is widely expressed in *Jtmt* endothelial cells and although the very small and delicate nature of the respiratory filtration barrier (particularly the < 2 μ m thick pulmonary endothelium) reduced the visualization quality of MT in this layer, preliminary results from the more sensitive competitive ELISA technique is encouraging. This method suggested that pulmonary endothelial cells from *Jtmt* mice carry at least a 2 fold increase in MT compared to FVB controls. These data strongly supported our claim that the human MT I/II transgene was successfully overexpressed in the endothelial cells of transgenic mice (Teiken, 2011).

The new mouse (called Jtmt) was successfully developed and is a remarkably effective model for mitigating BM thickening by crossing it with diabetic mice. In this regard it has been shown to completely eliminate hyperglycemia-driven GBM and myocardial capillary BM thickening, and it was the only known experimental protocol to fully mitigate diabetic BM thickening.

In light of preliminary studies showing that PABM was one of only a few BMs that are significantly widened in the diabetic OVE mouse (Carlson et al., 2003), the current Jtmt study utilized unbiased TEM morphometry to test my working hypothesis. The overall paradigm was designed to determine whether diabetes-induced oxidative stress might be a major factor in any possible PABM increased width, and secondly to determine the effect of MT overexpression in endothelial cells on PABM thickness.

The severely diabetic OVE mouse (Epstein et al., 1989) was chosen for the experimental model because early studies using this model of type I DM showed significant BM thickening in a wide variety of tissues including kidney (glomerulus), heart (myocardial capillaries), retina (choroid), lung, and peripheral nerves (Carlson et al., 2003, 2004, 2013). Although the lungs have not previously been implicated in chronic complications of DM, its highly vascularized parenchyma and potential for extensive oxidative damage warranted further study into potential hyperglycemia-driven PABM thickening.

To our knowledge, the current study was the first to report carefully applied morphometric methods to show PABM thickening in transgenic diabetic animals, and it was clearly the first to show that overexpression of MT in endothelial cells mitigated hyperglycemia-induced PABM thickening. Using a transgenic mouse line, we were able

to study DM in a remarkably long-living animal model (Carlson et al., 2013) that exhibits a plethora of pathophysiological features similar to those found in humans (Teiken et al., 2011). In addition, this model avoided any adverse effects of inducing diabetes in animals by the use of semi-toxic pharmaceutical drugs (e.g. streptozotcin) that may have serious side effects.

Our studies indicated that at 60 days of age, no significant differences were evident between PABM thickness in FVB, Jtmt and OVE, while OVEJtmt showed mildly thinner PABMs. This was undoubtedly due to the youth and immaturity of the mice when diabetes-induced complications were not manifested. Not surprisingly, light microscopy and TEM morphometric analysis showed no fundamental changes between the diabetic genotypes versus healthy controls. Additionally, a thorough investigation of BM thickness increases in other tissues at 60 days of age would be necessary to determine the approximate age of onset of vascular complications in diabetic mice.

On the contrary, at 150 days changes in PABM thickness between diabetic and healthy control mice were measurable and significant. Interestingly, the OVEJtmt bitransgenic mice showed a significantly reduced PABM thickening compared to the OVE and FVB lines. These data strongly supported the existing considerable evidence that ROS may be a primary cause for DM-induced BM thickening in various tissues, and that antioxidants, specifically MT, were effective scavengers of circulating free radicals in affected tissues.

In summary, data in the current study strongly support the working hypothesis of the current study that 1) PABMs exhibit DM-related thickening in severely diabetic mice

and 2) that this structural alteration is mitigated by specific endothelial targeted expression of MT.

These results offer much more than merely interesting data, and they clearly exhibit more than yet another instance of diabetic BM thickening. Because historically the lungs have not presented major clinical challenges in DM, experimental designs based on this organ have been largely ignored. As a consequence, the concept of diabetic pulmonopathy as one of the major chronic complications of DM has not reached the level of current conventional wisdom. Nevertheless, data in the current study provide unequivocal evidence that at 150 days of age, hyperglycemia-driven oxidative stress leads to statistically significant increased true width (+20%) of PABM in severely diabetic transgenic mice. More importantly, the study demonstrates that antioxidants specifically targeted to the global endothelial cell population completely eliminates hyperglycemia-driven PABM thickening and returns their width to below onset control levels. This is astonishing and places the PABM in a class of elite BMs including glomerular and myocardial capillary BMs that are reduced to normal width and respond positively to endothelial antioxidant therapy (Hewitt et al., abstract in press).

It is concluded that the current study provides a previously unknown baseline of morphometric information on PABM widths in control and severely diabetic transgenic mice and establishes a definition of diabetic pulmonopathy as a new and innovative chronic complication of diabetes. Moreover our preliminary data demonstrates the efficacy of antioxidant therapy on this disease and offers hope for translational studies by which this therapeutic modality can become a model for the reduction of the devastating consequences of many if not, all chronic complications of DM issues.

APPENDIX

Table 1. Animal genotype, number of animals, number of epoxy blocks sectioned, number of micrographs taken, and number of measurements made per micrograph for orthogonal intercept calculation of true PABM thickness.

| Genotype | Number of Animals | Total # of Blocks | Total # of Micrographs | Average # of PABM measurements per micrograph | Total # of PABM measurements |
|------------------|-------------------|-------------------|------------------------|---|------------------------------|
| 60 Day-Old Mice | | | | | |
| FVB | 6 | 12 | 120 | 7.49 | 899 |
| OVE | 6 | 12 | 129 | 7.78 | 1,004 |
| Jmt | 6 | 12 | 118 | 8.58 | 1,013 |
| OVEJmt | 6 | 11 | 118 | 8.79 | 1,038 |
| TOTAL | 24 | 47 | 485 | 8.15 | 3,954 |
| 150 Day-Old Mice | | | | | |
| FVB | 6 | 12 | 120 | 9.7 | 1,165 |
| OVE | 4 | 8 | 80 | 11.2 | 896 |
| Jmt | 7 | 14 | 137 | 8.75 | 1,199 |
| OVEJmt | 6 | 12 | 120 | 9.24 | 1,109 |
| TOTAL | 23 | 46 | 457 | 9.56 | 4,369 |

Numerical data derived from micrographs of 60 and 150 day-old mice, listed by genotype with the number of animals used for each group, as well as the total number of blocks sectioned, total number of micrographs taken, and the average number of measurements per micrograph. The final column lists the total number of micrographs obtained for each genotype.

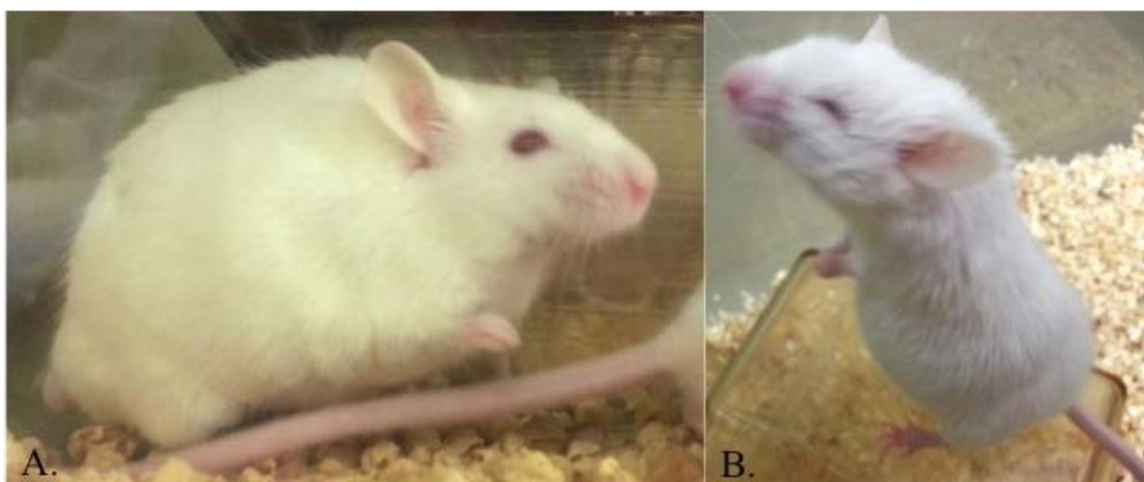


Figure 1. General appearance of 150 day-old mice.
A) Representative normal (FVB) mouse. FVB and transgenic (Jtmt) normal animals similar to this mouse can be identified by the presence of normal eyes.
B) Representative diabetic (OVE) mouse. OVE and bi-transgenic (OVEJtmt) diabetic mice consistently exhibit small eyes as illustrated.

Table 2. Mean body weight, blood glucose, and HbA1c values from 60 and 150 day-old FVB, Jtmt, OVE and OVEJtmt mice \pm S.D.

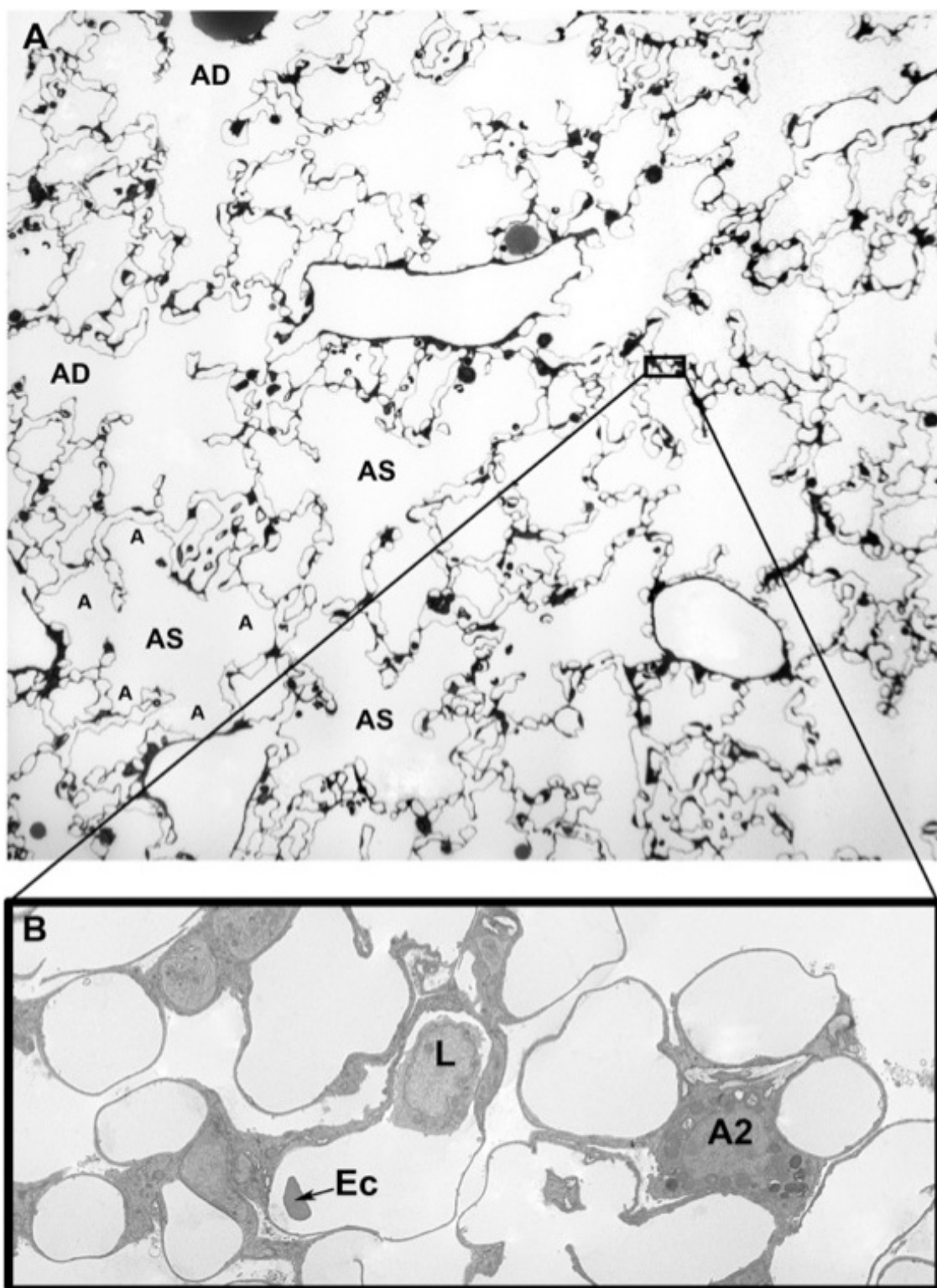
| Genotype | Age (days) | Body Wt (g) | Blood Glucose (mgs/dl) | HbA1c (%) |
|----------|------------|------------------|------------------------|------------------|
| FVB | 60 | 21.78 \pm 1.69 | 192.83 \pm 21.95 | 4.30 \pm 0.01 |
| FVB | 150 | 34.80 \pm 3.96 | 198.80 \pm 21.71 | 4.06 \pm 0.08 |
| Jtmt | 60 | 27.21 \pm 3.74 | 194.00 \pm 38.59 | 4.20 |
| Jtmt | 150 | 28.47 \pm 2.86 | 188.28 \pm 31.06 | <4.0 |
| OVE | 60 | 22.87 \pm 1.77 | 644.66 \pm 64.19 | 8.65 \pm 0.74 |
| OVE | 150 | 29.97 \pm 2.81 | 715.50 \pm 49.00 | 10.40 \pm 1.43 |
| OVEJtmt | 60 | 20.96 \pm 1.80 | 610.16 \pm 68.16 | 8.50 \pm 1.04 |
| OVEJtmt | 150 | 25.25 \pm 0.69 | 634.16 \pm 86.06 | 9.68 \pm 1.04 |

60 and 150 day-old mice listed by genotype and with their associated body weights (measured in grams), blood glucose levels (measured in mg/dl), and HbA1c levels (represented by percentages).

Figure 2. Toluidine blue stained light micrograph with higher magnification transmission electron micrograph inset of terminal respiratory region of 150 day-old FVB control mouse lung.

A) Light microscopic image of toluidine blue stained thick section of terminal respiratory portion of lung from FVB control mouse. Alveolar ducts (AD) and alveolar sacs (AS) dominate the field. Small rectangle indicates the area shown by TEM in the inset. x110.

B) Inset transmission electron micrograph illustrates pulmonary components typically located in the small rectangular region shown in figure 2A. A rich pulmonary capillary network separated from the air space by the respiratory filtration barrier is the primary feature of this region of the lung. Intravascular cells include lymphocytes (L) and erythrocytes (Ec) A type I alveolar cell (A2) is located in the respiratory septum between alveoli. X2,500.



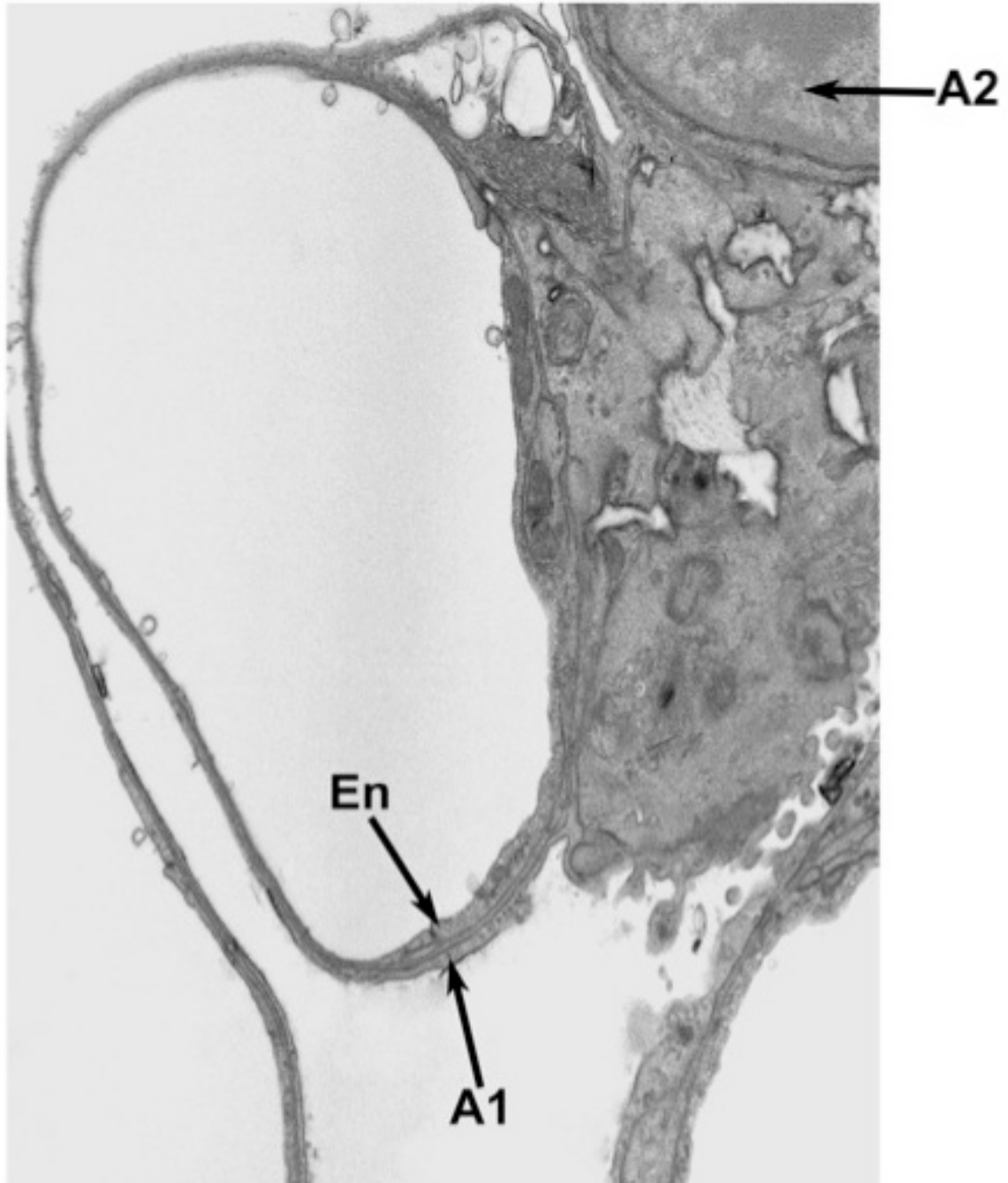


Figure 3. Transmission electron micrograph of 150 day-old FVB control mouse lung. Endothelial cells (En) line the inside of the blood-air barrier. Type I alveolar cells (A1) cover its external surface. Pulmonary alveolar basement membrane separated these two cells types. A type II alveolar cell (A2) is shown in the upper right corner of the micrograph. x16,000.

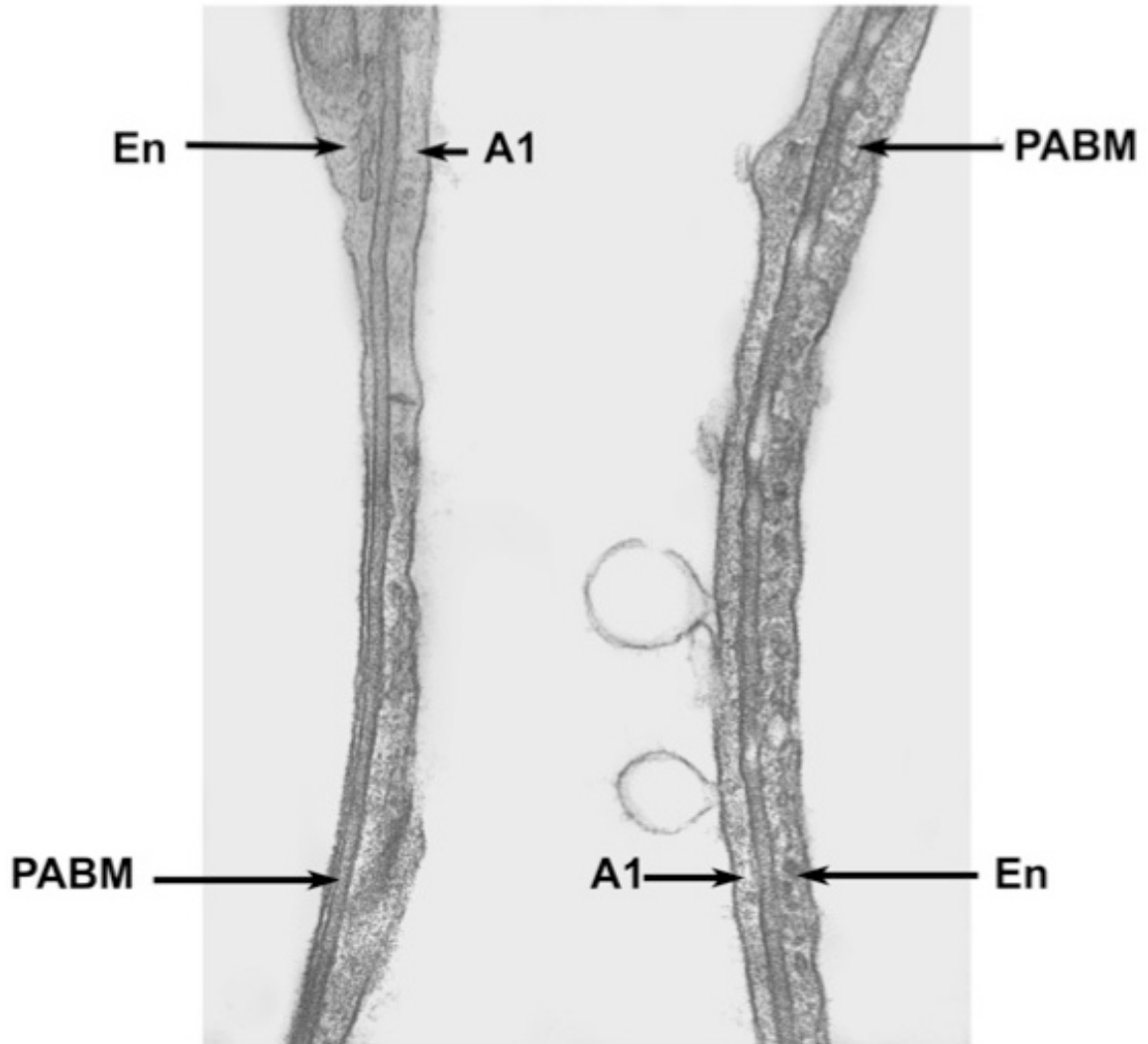


Figure 4. Transmission electron micrograph of two adjacent respiratory filtration barriers in lung of 150 day-old FVB control mouse. Endothelial cells (En) line the intravascular surface of the blood-air barrier, while type I alveolar cells (A1) line the air space of the barrier. The pulmonary alveolar basement membrane (PABM) is located between the two cell types and is indicated by the arrowhead. X60,000.

Figure 5. Representative transmission electron micrographs of respiratory filtration barriers in 60 day-old FVB, Jtmt, OVE, and OVEJtmt mice. Figures A-D illustrate typical blood-air barriers in FVB, Jtmt, OVE, and OVEJtmt mice at identical magnifications. Visual observation suggests that pulmonary alveolar basement membranes (located between opposing arrowheads) exhibit similar widths. x60,000.

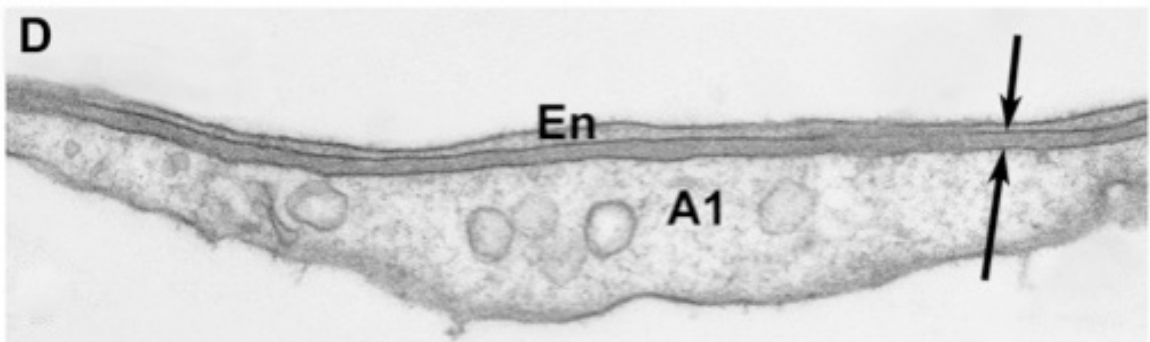
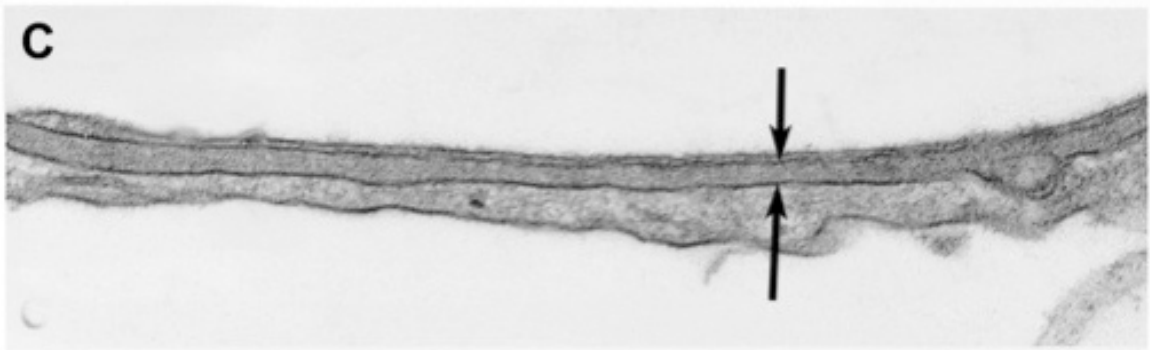
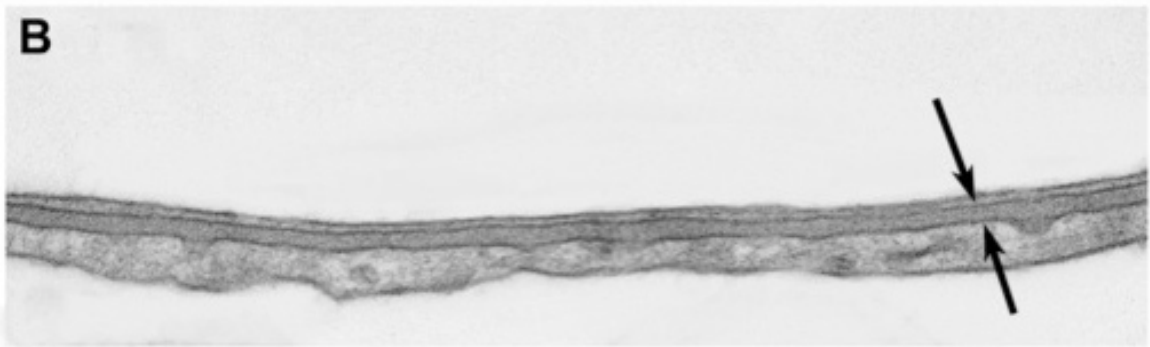
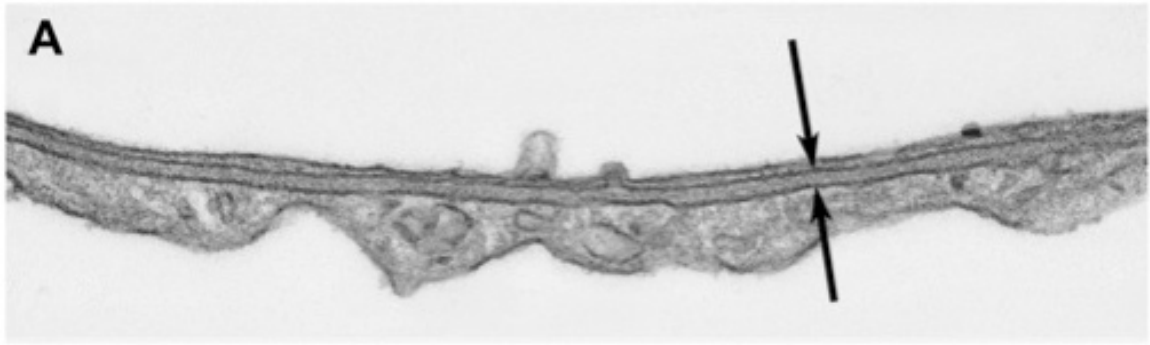
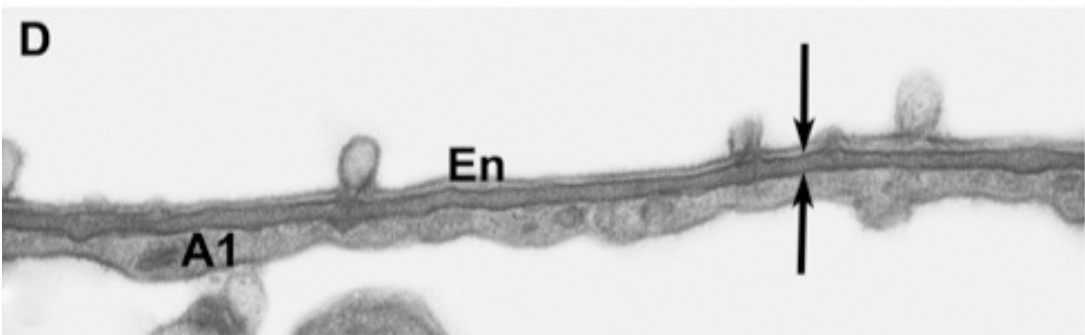
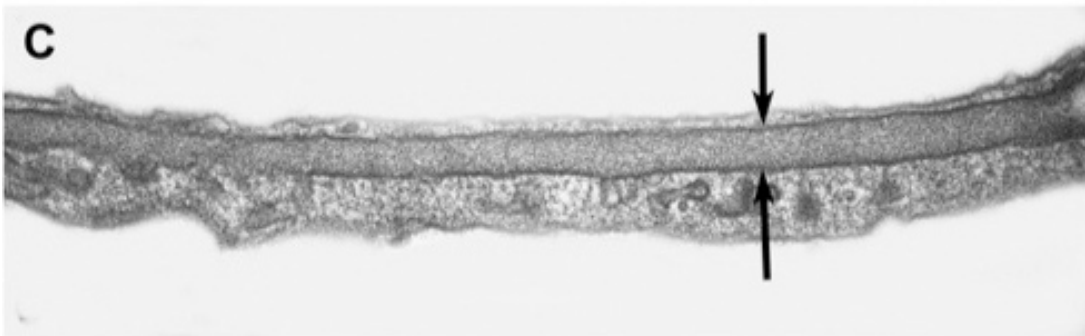
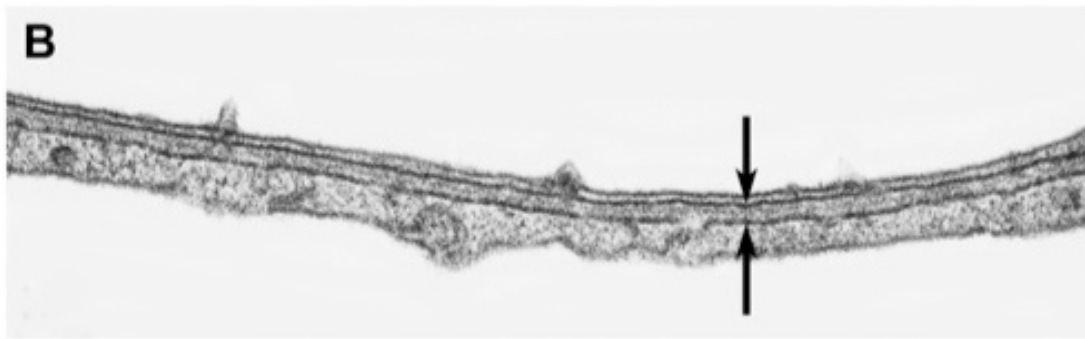


Figure 6. Representative transmission electron micrographs of respiratory filtration barriers in 150 day-old FVB, Jtmt, OVE, and OVEJtmt mice. Figures A-D illustrate typical blood-air barriers in FVB, Jtmt, OVE, and OVEJtmt mice at identical magnifications. Preliminary visual observations suggest that pulmonary alveolar basement membranes (located between opposing arrows) show similar thicknesses, except for the severely diabetic (OVE) animals indicated in Figure 5C. x60,000.



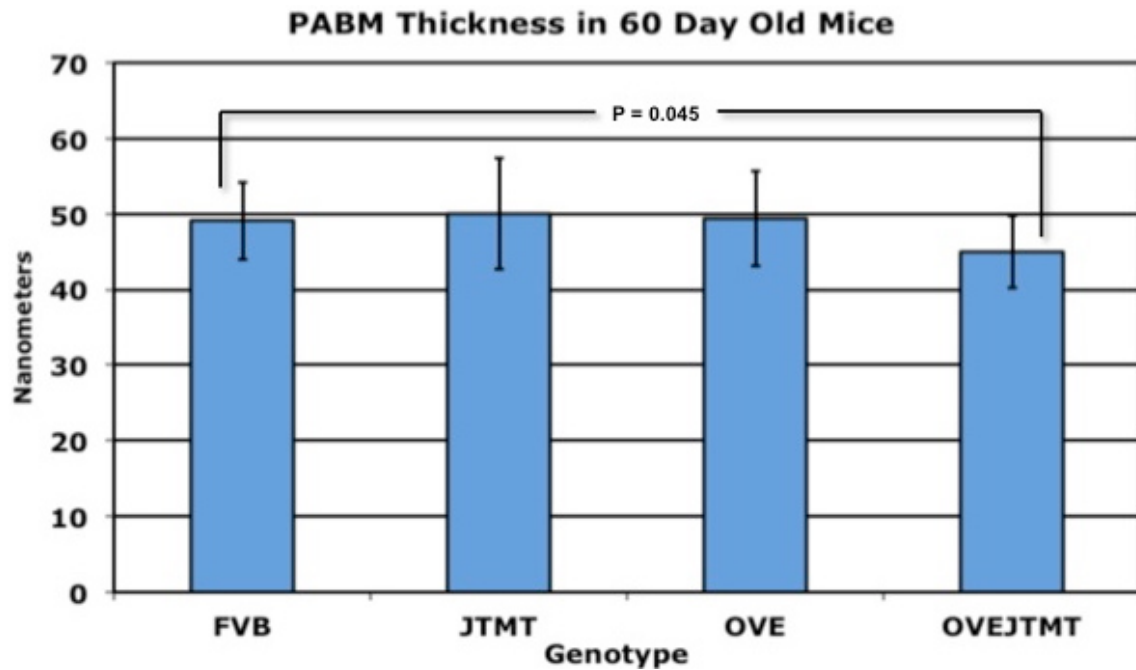


Figure 7. Mean pulmonary alveolar basement membrane thickness in 60 day-old mice. Non-transgenic background control mice (FVB), transgenic mice overexpressing metallothionein in endothelial cells (Jtmt), transgenic diabetic mice (OVE), and bi-transgenic diabetic mice overexpressing metallothionein in endothelial cells (OVEJtmt). FVB versus OVEJtmt show statistically significant differences. Statistically significant difference ($P < 0.05$).

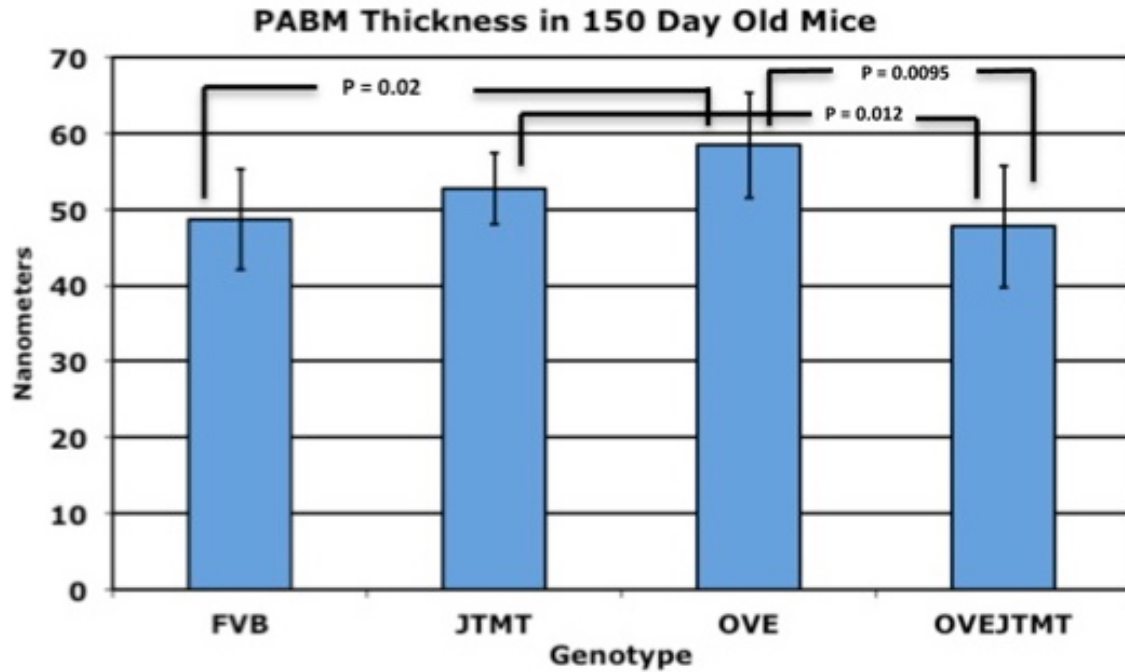


Figure 8. Mean pulmonary alveolar basement membrane thickness in 150 day-old mice. Non-transgenic background control mice (FVB), transgenic mice overexpressing metallothionein in endothelial cells (Jtmt), transgenic diabetic mice (OVE), and bi-transgenic diabetic mice overexpressing metallothionein in endothelial cells (OVEJtmt). FVB versus OVE, Jtmt versus OVEJtmt and OVE versus OVEJtmt show statistically significant differences. Statistically significant difference ($P < 0.05$).

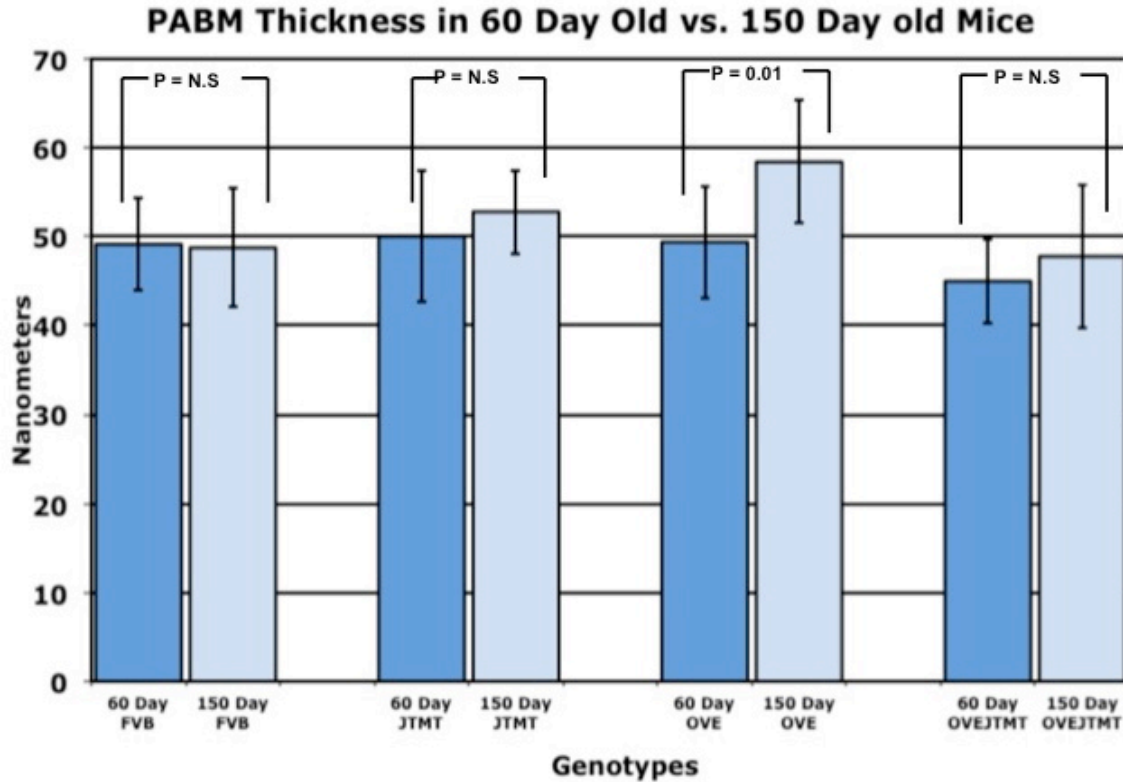


Figure 9. Age-related mean pulmonary alveolar basement membrane thickness in 60 day-old and 150 day-old mice. Statistical significance is shown between OVE 60 and 150 day-old mice ($P = 0.01$). P value is set at $p < 0.05$.

Table 3. Age-related mean pulmonary alveolar basement membrane thickness in 60 and 150 day-old mice.

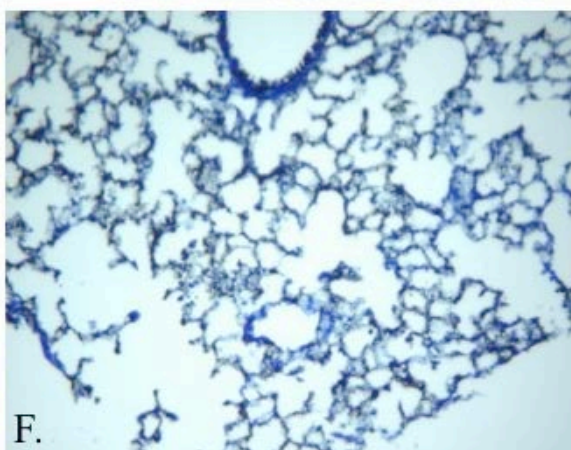
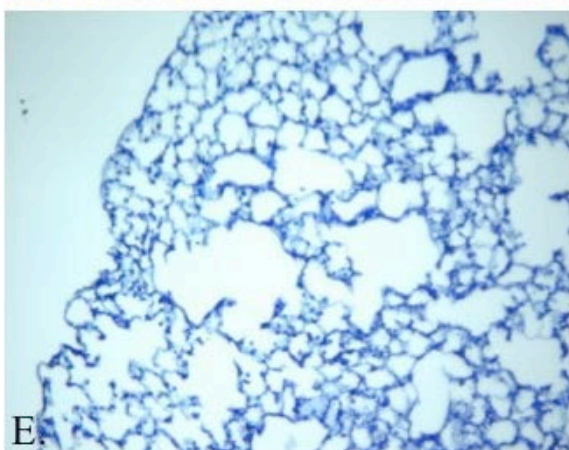
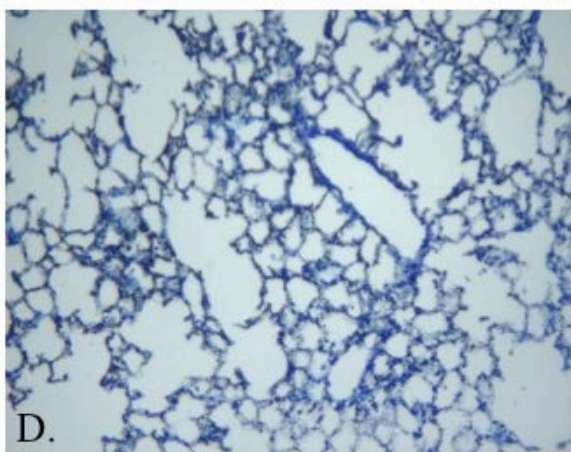
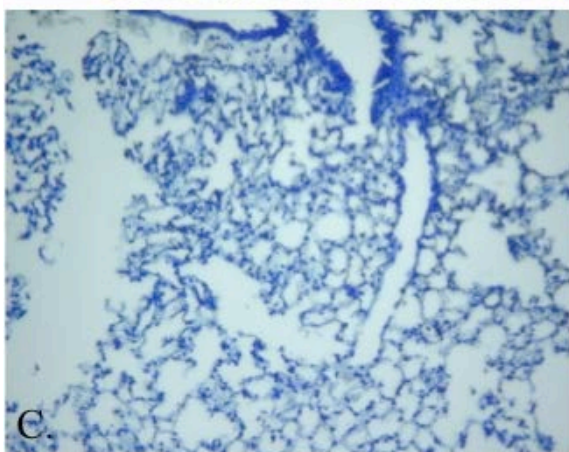
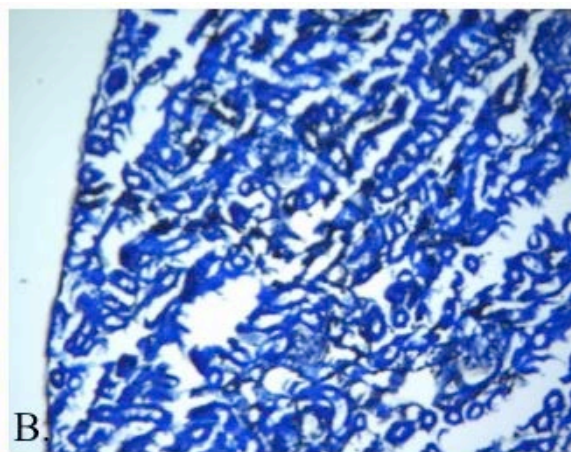
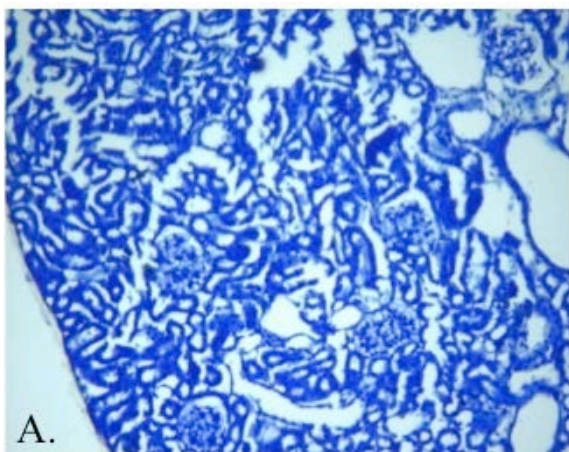
| Genotype | Age (Days) | Mean width +S.D. in nanometers | Age-related change in thickness | Age-related percentage change | Statistical Significance ($P < 0.05$) |
|----------|------------|--------------------------------------|---------------------------------------|-------------------------------------|---|
| FVB | 60 | 49.11 ± 5.13 | | | |
| FVB | 150 | 48.71 ± 6.63 | - 0.4 nm | - 0.8% | N.S. |
| Jtmt | 60 | 50.01 ± 7.38 | | | |
| Jtmt | 150 | 52.76 ± 4.79 | + 2.75 nm | + 5.4% | N.S. |
| OVE | 60 | 49.37 ± 6.29 | | | |
| OVE | 150 | 58.42 ± 6.93 | + 9.09 nm | + 18.3% | $P = 0.44$ |
| OVEJtmt | 60 | 44.97 ± 4.76 | | | |
| OVEJtmt | 150 | 47.75 ± 8.01 | + 2.78 | + 6.1% | N.S. |

Numerical comparison of pulmonary alveolar basement membrane thickness in 60 and 150 day-old non-transgenic background control mice (FVB), transgenic mice (Jtmt), transgenic diabetic mice (OVE), and bi-transgenic diabetic mice overexpressing metallothionein in endothelial cells (OVEJtmt) ± S.D.

Figure 10. Representative light micrographs of paraffin embedded kidney cortex and lung immunohistochemically stained for MTII.

- A) Jtmt kidney. Negative control; primary antibody omitted.
- B) Jtmt kidney
- C) FVB lung. Negative control, primary antibody omitted.
- D) FVB lung.
- E) Jtmt lung. Negative control, primary antibody omitted.
- F) Jtmt lung.

MT I/II staining was observed in proximal tubules of the kidney. Light staining was observed in the alveolar-capillary network of the FVB lung and more intense staining was observed in the Jtmt lung.



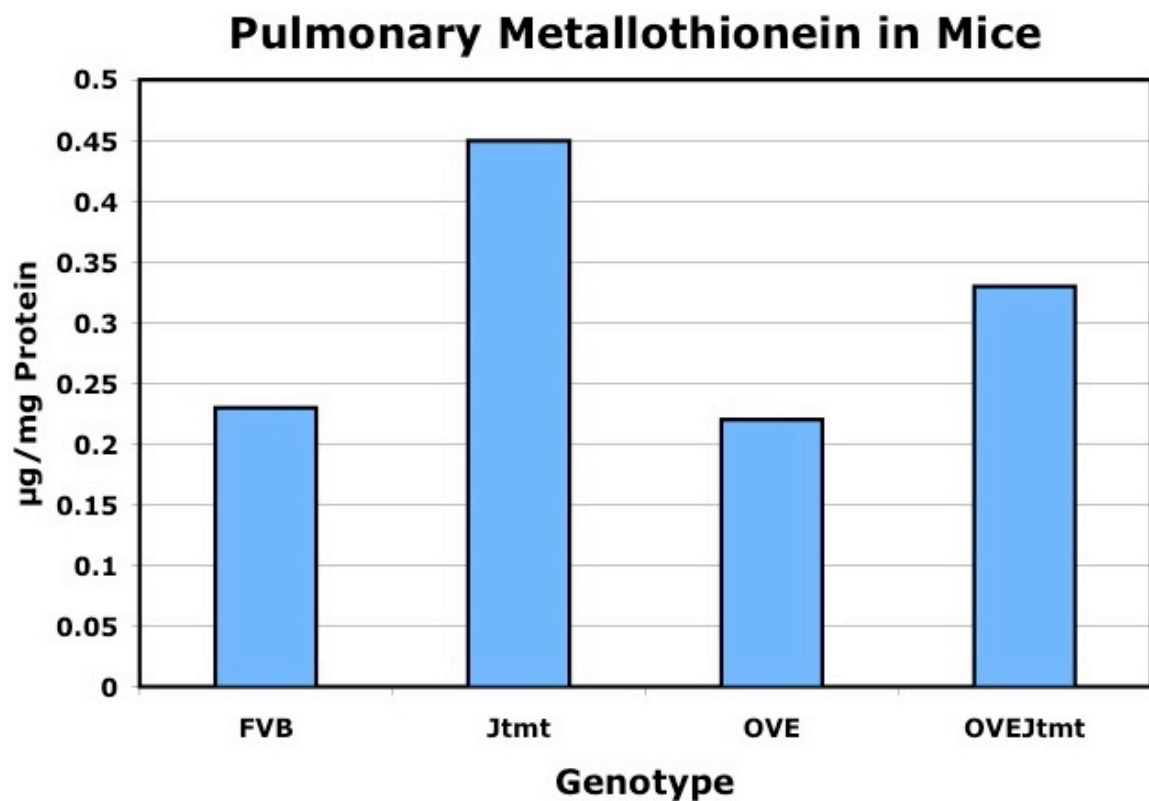


Figure 11. Average pulmonary MT I/II ($\mu\text{g}/\text{mg}$ total tissue protein) in FVB control (n=2), Jtmt transgenic (n=2), OVE (n=2) and OVEJtmt (n=2) transgenic and bi-transgenic animals. In Jtmt mice, MT I/II was approximately a two-fold increase over the FVB control. In the OVEJtmt MT I/II measured approximately 0.5 fold higher than the FVB control.

REFERENCES

- Apparao K, Newman D, Zhang H, Khosla J, Randell S, Sannes P. 2010. Temporal changes in expression of FoxA1 and Wnt7A in isolated adult human alveolar cells enhanced by heparin. *The Anatomical Record* 293 (938:946).
- Bauer P.S. and Stacey T.R. 1977. The use of PIPES bugger in the fixation of mammalian and marine tissues for electron microscopy. *J Microsc*, 109(3), 315-327.
- Bergstrand A and Bucht H. 1959. The glomerular lesions of diabetes mellitus and their electron-microscope appearances. *J Pathol Bacteriol* 77(1):231-42.
- Bloom W and Fawcett DW. 1986. Respiratory system. In: *A textbook of histology*. 11th ed. Philadelphia, PA: Elsevier Health Sciences. 629 p.
- Bradford, M. M. 1976. A rapid and sensitive method for the quantitation of microgram quantities of protein utilizing the principle of protein-dye binding. *Anal Biochem*, 72, 248-254.
- Brownlee M. 2001. Biochemistry and molecular cell biology of diabetic complications. *Nature* 414(December):813-20.
- Cai L. 2004. Metallothionein as an adaptive protein prevents diabetes and its toxicity. *Nonlinearity in Biology, Toxicology, and Medicine* 2:89-103.
- Carlson EC, Vari RC, Audette JL, Finke MA, Ressler MJ. 2004. Significant glomerular basement membrane thickening in hyperglycemic and normoglycemic diabetic-prone BB wistar rats. *Anat Rec A Discov Mol Cell Evol Biol* 281(2):1308-18.
- Carlson EC, Audette JL, Veitenheimer NJ, Risan JA, Laturus DI, Epstein PN. 2003. Ultrastructural morphometry of capillary basement membrane thickness in normal and transgenic diabetic mice. *The Anatomical Record* (271 A):332-341.
- Carlson EC, Chhoun JM, Laturus DL, Bikash KC, Berg B, Zheng S, Epstein PN. 2013. Podocyte-specific overexpression of metallothionein mitigates diabetic complications in the glomerular filtration barrier and glomerular histoarchitecture: A transmission electron microscopy stereometric analysis. *Diabetes Metab Res Rev* 29(2):113-24.

- Centers for Disease Control and Prevention. National diabetes fact sheet: national estimates and general information on diabetes and prediabetes in the United States, 2011. Atlanta, GA: U.S. Department of Health and Human Services, Centers for Disease Control and Prevention, 2011.
- Chen H, Carlson EC, Pellet L, Moritz JT, Epstein PN. 2001. Overexpression of metallothionein in pancreatic beta-cells reduces streptozotocin-induced DNA damage and diabetes. *Diabetes* 50(9):2040-6.
- Cross P and Mercer K. 1993. Respiratory system. In: *Cell and tissue ultrastructure: A functional perspective*. New York: W. H. Freeman and Company. 303 p.
- Dische FE. 1992. Measurement of glomerular basement membrane thickness and its application to the diagnosis of thin-membrane nephropathy. *Arch Pathol Lab Med* 116(1):43-9.
- Epstein PN, Overbeek PA, Means AR. 1989. Calmodulin-induced early-onset diabetes in transgenic mice. *Cell* 58(6):1067-73.
- Epstein PN, Ribar TJ, Decker GL, Yaney G, Means AR. 1992. Elevated beta-cell calmodulin produces a unique insulin secretory defect in transgenic mice. *Endocrinology* 130(3):1387-93.
- Evans MJ, Fanucchi MV, Plopper CG, Hyde DM. 2010. Postnatal development of the lamina reticularis in primate airways. *Anat Rec (Hoboken)* 293(6):947-54.
- Fuso L, Cotroneo P, Basso S, De Rosa M, Manto A, Ghirlanda G, Pistelli R. 1996. Postural variations of pulmonary diffusing capacity in insulin-dependent diabetes mellitus. *Chest* 110(4):1009-13.
- Goh and Cooper. 2008. The role of advanced glycation end products in progression and complications of diabetes. *J Clin Endocrinol Metab* 93(4):1143-1152.
- Gundersen HJ and Osterby R. 1973. Statistical analysis of transformations leading to normal distribution of measurements of the peripheral glomerular basement membrane. *J Microsc* 97(3):293-9.
- Hewitt H, Bowker W, Laturus D, Albrecht K, Young K, Chhoun J, Epstein P, and Carlson E. Endothelial cell specific targeting of metallothionein eliminates myocardial capillary, glomerular, and pulmonary alveolar basement membrane thickening in OVE transgenic diabetic mice. Abstract in Press. 2013.
- Hirose K, Osterby R, Nozawa M, Gundersen HJ. 1982. Development of glomerular lesions in experimental long-term diabetes in the rat. *Kidney Int* 21(5):689-95.

- Jahromi MM and Eisenbarth GS. 2007. Cellular and molecular pathogenesis of type 1A diabetes. *Cell Mol Life Sci* 7:865-72.
- Jensen EB, Gundersen HJ, Osterby R. 1979. Determination of membrane thickness distribution from orthogonal intercepts. *J Microsc* 115(1):19-33.
- Kalluri R. 2003. Basement membranes: Structure, assembly and role in tumour angiogenesis. *Nature Reviews* 3(June):422-33.
- Kida K, Utsuyama M, Takizawa T, Thurlbeck WM. 1983. Changes in lung morphologic features and elasticity caused by streptozotocin-induced diabetes mellitus in growing rats. *Am Rev Respir Dis* 128(1):125-31.
- Kimmelstiel P. Wilson, MB. 1936. Intercapillary lesions in the glomeruli of the kidney. *Am J Pathol* 12:83-98.
- Kumari MV, Hiramatsu M, Ebadi M. 1998. Free radical scavenging actions of metallothionein isoforms I and II. *Free Radic Res* 29(2):93-101.
- LeBleu VS, MacDonald B, Kalluri R. 2007. Structure and function of basement membranes. *Exp Biol Med* 232:1121-9.
- Liang Q, Carlson EC, Donthi RV, Kralik PM, Shen X, Epstein PN. 2002. Overexpression of metallothionein reduces diabetic cardiomyopathy. *Diabetes* 51:174-81.
- Madonna R and De Caterina RD. 2011. Cellular and molecular mechanisms of vascular injury in diabetes - part I: Pathways of vascular disease in diabetes. *Vascular Pharmacology* 54:68-74.
- Madonna R and De Caterina RD. 2011. Cellular and molecular mechanisms of vascular injury in diabetes - part II: Cellular mechanisms and therapeutic targets. *Vascular Pharmacology* 54:75-9.
- Mason RM and Wahab NA. 2003. Extracellular matrix metabolism in diabetic nephropathy. *J Am Soc Nephrol* 14(5):1358-73.
- McCance K and Heuther S. 2010. Dysfunction of the endocrine pancreas: Diabetes Mellitus. In: *Pathophysiology: The biologic basis for disease in adults and children*. Clark S, Brashers V, Rote N, editors. 6th ed. Maryland Heights, Missouri: Mosby Elsevier. 745 p.
- Meyer, M. 2006. Decreased renal basement membrane thickening is accompanied by elevated renal antioxidants in the Aimes dwarf mouse model of delayed aging. Doctoral Dissertation. Located at: the University of North Dakota School of Medicine and Health Sciences.

- Monnier VM, Kohn RR, and Cerami A. 1984. Accelerated age-related browning of human collagen in diabetes mellitus. *Proc Natl Acad Sci*. 81(2): 583-587.
- Nishikawa T, Edelstein D, Brownlee M. 2000. The missing link: A single unifying mechanism for diabetic complications. *Kidney Int Suppl* 77(Sept):S26-30.
- Nokoff N and Rewers M. 2013. Pathogenesis of type I diabetes: Lessons from natural history studies of high-risk individuals. *Ann N Y Acad Sci* 1291(The Year in Diabetes and Obesity):1-15.
- Ofulu AF, Kida K, Thurlbeck WM. 1988. Experimental diabetes and the lung. I. changes in growth, morphometry, and biochemistry. *Am Rev Respir Dis* 137(1):162-6.
- Ofulue AF and Thurlbeck WM. 1988. Experimental diabetes and the lung. II. in vivo connective tissue metabolism. *Am Rev Respir Dis* 138(2):284-9.
- Ozsahin K, Tugrul A, Mert S, Yuksel M, Tugrul G. 2006. Evaluation of pulmonary alveolo-capillary permeability in type 2 diabetes mellitus: Using technetium 99mTc-DTPA aerosol scintigraphy and carbon monoxide diffusion capacity. *J Diabetes Complications* 20(4):205-9.
- Rains JL and Jain SK. 2011. Oxidative stress, insulin signaling, and diabetes. *Free Radical Biology & Medicine* 50:567-75.
- Richer MJ and Horwitz MS. Viral infections in the pathogenesis of autoimmune diseases: focus on type 1 diabetes. *Front Biosci*. 2008 May 1;13:4241-57. Review.
- Rohrbach DH and Martin GR. Structure of Basement Membrane in Normal and Diabetic Tissue. *Annals New York Academy of Sciences*. 1982;82:203-211.
- Sato M and Bremner I. 199. Oxygen free radicals and metallothionein. *Free Radic Bio Med* 14(3):325-37.
- Schmidt AM, Yan SD, Yan SF, Stern DM. 2000. The biology of the receptor for advanced glycation end products and its ligands. *BBA Molecular Cell Research* 1498(2-3):99-111.
- Shafiee G, Khamseh M, Rezaei N, Aghili R, Malek M. 2013. Alteration of pulmonary function in diabetic nephropathy. *Journal of Diabetes & Metabolic Disorders* 12(15).
- Sheetz MJ and King GL. 2002. Molecular understanding of hyperglycemia's adverse effects for diabetic complications. *Jama* 288(20):2579-88.
- Smits NC, Shworak NW, Dekhuijzen PNR, Van Kuppevelt TH. 2010. Heparan sulfates in the lung: Structure, diversity, and role in pulmonary emphysema. *The Anatomical Record* 293:955-67.

- Son SM. 2007. Role of vascular reactive oxygen species in development of vascular abnormalities in diabetes. *Diabetes Research and Clinical Practice* 77S:S65-70.
- Sorokin SP. The respiratory system. 1988. Leon Weiss, editor. In: *Cell and tissue biology a textbook of histology: 6th edition* Baltimore: Urban and Schwarzenberg. p 753-813.
- Suzuki Y, Churg J, Grishman E, Mautner W, Dachs S. 1963. The mesangium of the renal glomerulus: Electron microscopic studies of pathologic alterations. *Am J Pathol* 43:555-78.
- Taketo M, Schroeder A, Mobraaten L, Gunning K, Hanten G, Fox R, Roderick T, Stewart C, Lilly F, Hansen C, et al. 1991. FVB/N: An inbred mouse strain preferable for transgenic analysis. *Proc Natl Acad Sci USA* 88:2065-2069.
- Teiken J. 2011. Production of a transgenic mouse that specifically overexpresses the antioxidant metallothionein in endothelial cells. Doctoral Dissertation. Located at: University of North Dakota School of Medicine and Health Sciences.
- Teiken JM, Epstein PN, Carlson EC. TEM stereometric analysis of glomeruli in aging OVE26 transgenic diabetic mice. 2011. *Am J Nephrol.* 33 Suppl 1:8-14.
- Thirumoorthy N, Sunder AS, Manisenthil Kumar KT, Senthil Kumar M, Ganesh GNK, Chatterjee M. 2011. A review of metallothionein isoforms and their role in pathophysiology. *World Journal of Surgical Oncology* 9(54):1-7.
- Tsilibary EC. 2003. Microvascular basement membranes in diabetes mellitus. *J Pathol* 200:537-46.
- Velic A, Laturus D, Chhoun J, Zheng S, Epstein P, Carlson E. 2013. Diabetic basement membrane thickening does not occur in myocardial capillaries of transgenic mice when metallothionein is overexpressed in cardiac myocytes. *Anat Rec (Hoboken)* 296(3):480-7.
- Venable JH and Coggeshall R. 1965. A simplified lead stain for use in electron microscopy. *J. Cell Biol.*, 25:407-408.
- Viberti G, Wiseman M, Pinto J, Messent J. Diabetic Nephropathy in Joslin's Diabetes Mellitus 13th edition. 1994 Edited by Kahn CR, Weir GC. Lea and Febiger: Philadelphia, PA 691-737
- Vracko R. 1976. Effects of aging and diabetes on basal lamina thickness of six cell types. In: *Biology and chemistry of basement membranes*. Kefalides NA, editor. 1st ed. New York, New York: Academic press. 483 p.

- Vracko R, Thorning D, Huang TW. 1979. Basal lamina of alveolar epithelium and capillaries: Quantitative changes with aging and in diabetes mellitus. *Am Rev Respir Dis* 120(5):973-83.
- Watanabe K, Senju S, Toyoshima H, Yoshida M. 1997. Thickness of the basement membrane of bronchial epithelial cells in lung diseases as determined by transbronchial biopsy. *Respiratory Medicine* 91:406-10.
- Wild S, Roglic G, Green A, Sicree R, King H. 2004. Global prevalence of diabetes: Estimates for the year 2000 and projections for 2030. *Diabetes Care* 27(5):1047-53.
- World Health Organization. 2006. Definition and diagnosis of diabetes mellitus and intermediate hyperglycemia: Report of a WHO/IDF consultation.
- Wright JR E, Scism-Bacon JL, Glass LC. 2006. Oxidative stress in type 2 diabetes: The role of fasting and postprandial glycaemia. *Int J Clin Pract* 60(3):308-14.
- Yurchenco PD and Patton BL. 2009. Developmental and pathogenic mechanisms of basement membrane assembly. *Curr Pharm Des* 15(12):1277-94.
- Zamboni L and Stefanini M. 1968. On the configuration of the plasma membrane of the mature spermatozoon. *Fertil Steril* 19(4):570-9.
- Zheng S, Carlson EC, Yang L, Kralik PM, Huang Y, Epstein PN. 2008. Podocyte-specific overexpression of the antioxidant metallothionein reduces diabetic nephropathy. *J Am Soc Nephrol* 19(11):2077-85.